UiT The Arctic University of Norway

Faculty of Science and Technology
Department of Mathematics and Statistics

An Energy Balance Model on an Infinite Line

Ask Elvevold

MAT-3941 Master's thesis in applied physics and mathematics - 30 ECTS
June 2022

Contents

1 Introduction

Climate modelling is a large field of applied mathematics, and in the current global state it plays a significant role in the future of the planet. Climate models can be used to predict how the climate will respond to different forcings and help aid in deciding what measures are needed to be taken to reduce the negative effects of climate change. There are many different models that are used to make these analyses but hiding in the depths below all of it is almost always a form of energy balance. The model analysed in this thesis was originally proposed by Budyko [1] in 1969, and further investigated by North [2] in 1975. The objective of this thesis was to investigate what the bistability of Norths model is dependent upon, by analysing a similar model. The analysis entails finding stationary solutions using a boundary formulation of the model, computing the bifurcation diagram as a function of the solar irradiation constant, and assessing their stability using numerical methods. The goal is not to find a model that more accurately represents the climate on earth, but rather investigate the behaviour of the model under different circumstances. In Norths analysis, a constant heat diffusion coefficient was used on the entire globe. However, by allowing different regions of the line to have different heat diffusion coefficients, more complicated behaviour is allowed to occur. Two cases were investigated, the first assumes constant heat diffusion on the entire line, which is what North did. This case gave a bistability with an unstable solution in between, which is similar to what North found. In the second case the heat diffusion coefficient was allowed to change on the line, which lead to much more intricate behaviour. It gave rise to spontaneous symmetry breaking, a possibility of having infinitely many solutions for a specific value of input radiation, and a similar bistability to the case with constant heat diffusion in certain conditions.

2 Model

The model used in the analysis is similar to that of North, with the key distinction that it is considered on the unbounded real axis, contrary to only on a half sphere. This means that the variable that described the sine of the latitude x in Norths model now simply describes the position in units of earth radii. The energy input on the line is a function $S(x)$, with a few restrictions. $S(x)$ is symmetric around $x = 0$, it has its only local maximum at $x = 0$, and it's integral over the real line is finite. Now this function determines both the total energy input on the line, and how it's distributed on different points on the line. In the model it is multiplied with the solar irradiation constant Q and a term involving the albedo of earth, $(1 - a)$, determining the rate of radiation absorption. The solar radiation constant is constant, while the albedo is allowed to change on the line, modelling how different surfaces reflect sunlight differently. For example, ice and snow reflects radiation differently to water and land does, this is modelled by

$$a(T) = \begin{cases} a_0, & T < -10°C, \text{ no continent at } x \\ a_1, & T > -10°C, \text{ no continent at } x \\ a_0, & T < 0°C, \text{ continent at } x \\ a_1, & T > 0°C, \text{ continent at } x \end{cases} \quad (1)$$

With $a_0 = 0.6$ and $a_1 = 0.38$. This function introduces the concept of continents, which is an extension of the North model. What continents allow is to change the melting-point of snow/ice and the heat diffusion coefficient over different regions of the line. This is to model the fact that water on land is generally freshwater, which melts at 0 degrees Celsius, while seawater is a mixture of salt and water and thus has a much lower freezing point, here -10 degrees Celsius. And also to model how diffusive heat transport works differently over land than it does over the sea.

The earth will also radiate energy based on its temperature due to blackbody radiation. This is usually a highly nonlinear term (T^4), but like Budyko did, this can be modelled within reasonable errors by the empirical formula

$$I = A + BT \quad (2)$$

Where I is the outgoing radiation due to blackbody radiation, $A = 192.2\frac{W}{m^2}$ and $B = 3.85\frac{W}{°Cm^2}$. This is a linearization of how the surface temperature affect the blackbody radiation of earth. It is important to note that the radiation is not determined by the temperature at the surface, but rather the temperature high up in the atmosphere. This model does assume that there is a linear dependence between the surface temperature and the temperature high in the atmosphere that determines the outgoing radiation. The linearization is in powers of $°C/273$, which makes the error of linearization acceptable for the temperatures of interest in the model. In Norths analysis it was found to have an error of less 1% in the temperatures of interest in the modelling[2]. Combining this with the assumed diffusive heat transport, the model takes the form of a non-linear partial differential equation.

$$C\partial_t T - \partial_x K(x)\partial_x T + BT = QS(x)(1 - a(T)) - A \quad (3)$$

Where $C = 13.2\frac{sW}{°Cm^2}$, Q has units $\frac{W}{m^2}$ and is left as variable in the model, and $K(x)$ has units of $\frac{W}{°C}$. In the model, the $K(x)$ parameter has already absorbed the spatial scaling, leaving the variable x with units of earth radii. The function is modelled as a step function, having distinct constant values in regions with a continent and regions without.

$$K(x) = \begin{cases} K_w, & \text{no continent at } x \\ K_l, & \text{continent at } x \end{cases} \quad (4)$$

Where $K_w = 0.38\frac{W}{°C}$ and $K_l = 1.89\frac{W}{°C}$.

The C parameter contains the time-scale of the model, and its value is chosen such that the variable t in the model has units of half-years based upon empirical measurements of how long the climate takes to react to a perturbation of its stable case[3]. However, it's value is not significant in this analysis, as the main goal is to investigate the bistability of the model, not its real-world

accuracy. The parameters K_w and K_l are chosen to be close to what North found in his analysis. The key difference is that North had a singular heat diffusion coefficient on the entire globe, while here it is allowed to change. $K_l > K_w$ means that it is assumed that heat dissipates more rapidly over continents than it will over the sea. This assumption might not hold in the real-world, as it is suspected that the main action causing heat diffusion over the globe is wind. And wind speeds are generally higher over areas covered in water or ice than it is over continental areas where it is usually slowed down by vegetation and mountains. The reason it was still decided to keep K_l higher than K_w was that it highlights incredibly interesting behaviour of the model, and that aligns much better with the goal of this analysis than attempting to get an accurate climate model of the earth would. A more detailed derivation of the model can be found in appendix A.

The model in question here is a non-linear partial differential equation, with the exception being the case where the critical melting temperature is never crossed, which would make $a(T) = a_0$. For that special case, it might be possible to solve analytically. In fact, considering the case with no continent on the line, the function $K(x) = K_w$ will also be constant. Thus, simplifying the model down to

$$CT_t - K_w T_{xx} + BT = QS(x)(1 - a_0) - A \tag{5}$$

which can be solved analytically using a spectral method.

2.1 Analytical solution to special case

To solve the problem, using the normalized definition of the continuous Fourier transform (CFT) of a function $f(x)$,

$$F(k) = \frac{1}{\sqrt{2\pi}} \int_{-\infty}^{\infty} dx f(x) e^{-ikx} \tag{6}$$

with the corresponding inverse transform

$$f(x) = \frac{1}{\sqrt{2\pi}} \int_{-\infty}^{\infty} dk F(k) e^{ikx} \tag{7}$$

These definitions are according to how they are defined in Mathematica[4]. Performing this transform on the simplified model in equation (5) gives

$$CG_t + (k^2 K + B)G = QS^*(1 - a_0) - \sqrt{2\pi} A\delta(k). \tag{8}$$

Where G denotes the CFT of T, and S^* the CFT of S, all with respect to x. This is a first order ODE, and it has solution

$$G(k,t) = e^{-\frac{t(B-k^2K)}{C}} \left(c_1 - \frac{(a_0 - 1)e^{-\frac{t(B-k^2K)}{C}} QS^*(k)}{B + k^2 K} - \frac{e^{\frac{tB}{C}} \sqrt{2\pi} A\delta(k)}{B} \right) \tag{9}$$

Where c_1 can determined by an initial condition on $T(x,0)$, which then equates to an initial condition on $G(k,0)$. The solution $T(x,t)$ can be computed by doing the inverse CFT of the above expression. Unfortunately, all the interesting behaviour of the model happens in cases where the thresholds in $a(T)$ are crossed, and this special case does not give much insight into that behaviour. It can however be useful for verifying the validity of the numerical methods that are used to solve the model in the next section. This solution assumes that $T(x,t) < -10°C$ for all x and t thus making $a(T) = a_0$, note that another way to get a similar solution would be if $T(x,t) > -10°C$ making $a(T) = a_1$. However, this will never have solutions that successfully converge to a stable state before breaking that very assumption, and this is due to the restriction put on $S(x)$. The requirement of having a bounded integral over the real line along with having $S(x) >= 0$ implies that it must go to zero at both ends toward infinity. Thus when $|x| >> 0$, $S(x) \approx 0$. Which simplifies the model into

$$-K_w T_{xx} + BT = -A \tag{10}$$

Where $T_t = 0$ and $T(x)$ is no longer a function of t as it is a stationary solution. This is a simple linear ODE and has general solution

$$T(x) = -\frac{A}{B} + c_1 e^{\sqrt{\frac{b}{k}}x} + c_2 e^{-\sqrt{\frac{b}{k}}x} \tag{11}$$

If this is on considered on far to the right on the line, where $x >> 0$ and thus $S(x) \approx 0$, c_1 has to be 0 to keep $T(x)$ a bounded function toward infinity, similarly for c_2 on the far left side. Thus making T fulfil the limits

$$\lim_{x \to \pm\infty} T(x) = -\frac{A}{B} \approx -49.92°C \tag{12}$$

These limits are completely independent upon initial conditions, meaning that the assumption $T(x,t) > -10°C$ will be broken before the solution reaches its equilibrium state. Nonetheless, with initial conditions $T(x,0) > -10°C$, the solution will be valid for some short period before it inevitably breaks.

3 Numerical methods

As mentioned earlier, when the $a(T)$ function cannot be simplified to a constant, the model is non-linear and extremely difficult to solve analytically. However, numerical methods can do this with ease, in this section two different numerical schemes to solve this model will be derived. One spectral method, and one finite difference method.

3.1 Spectral scheme

This section will solve a slightly altered version of the model

$$CT_t - K_w T_{xx} + BT = QS(x)(1 - a(T)) - A + \partial_x \hat{K}(x) \partial_x T \tag{13}$$

Where $K(x) = K_w + \hat{K}(x)$. To simplify a little bit, the right hand side of the model is simplified to $F(T)$, such that

$$F(T) = QS(x)(1 - a(T)) - A + \partial_x \hat{K}(x) \partial_x T \tag{14}$$

Which gives the altered model for the spectral case

$$CT_t - K_w T_{xx} + BT = F(T) \tag{15}$$

Now, to set up a spectral scheme for the problem, the model must be converted to its spectral form. Computing the CFT of the model in equation (15) gives

$$CG_t + (K_w k^2 + B)G = \mathcal{F}\{F(T)\} \tag{16}$$

Where G is the CFT of T, and $\mathcal{F}\{\cdot\}$ denotes the CFT of its content, all with respect to x. Rearranging a little bit gives

$$CG_t = \mathcal{F}\{F(T)\} - (K_w k^2 + B)G \tag{17}$$

This is a prime subject to solve using numerical ODE solving methods. The problem is that doing so requires both discretization of the line and reducing the domain of the solution to a finite segment of the line. This might make any results in the chosen domain be inaccurate, this can be investigated by comparing to the analytical solution in equation (9). Another issue that might occur is overlooking important behaviour of the model in regions outside the chosen domain, however choosing the right domain avoids this problem entirely. Due to the chosen $S(x)$-functions made later, a fitting restriction of the infinite line is to reduce it to $[-L, L]$ in the spatial domain and $[-K, K]$ in the spectral domain. Then choosing L large enough such $S(x)$ is sufficiently small at $|x| = L$. This will both ensure that the interesting parts of the solution is contained within the discretized spatial domain, and make the convergence in the spectral domain better. The discretization is done using N equidistant samples in both spatial and spectral domain according to

$$x_i = -L + i\frac{2L}{N} \qquad i = 0, 1, 2, \ldots, N-1 \tag{18}$$

$$k_i = -K + i\frac{2K}{N} \qquad i = 0, 1, 2, \ldots, N-1 \tag{19}$$

Where $K = \frac{\pi N}{2L}$. This scaling of the spectral domain is made such that the discrete Fourier transform (DFT) using discretized input approximates the CFT with continuous input[5]. The DFT of a series of samples $\{x_n\} = x_0, x_1, \ldots, x_{N-1}$ is $\{X_j\} = X_0, X_1, \ldots, X_{N-1}$ and is given by

$$X_j = c_0 \sum_{n=0}^{N-1} x_n e^{-i2\pi jn/N} \tag{20}$$

Where c_0 is a scaling parameter that changes on convention. Using this, sampling a function $f(x)$ using the discretization described in equations (18) and (19) an approximation of the CFT of $f(x)$ is

$$F(k_i) \approx c_0^* X_i \tag{21}$$

Where $F(k_i)$ is the CFT of $f(x)$ evaluated at the point $k = k_i$, X_i is the i'th sample in the DFT of the discretized data $\{x_n\} = f(x_0), f(x_1), \ldots, f(x_{N-1})$, and c_0^* is a scaling parameter that changes for different implementations of the algorithm that computes the DFT. In addition to this, it is also required to compute the inverse transform (IDFT) for each step, and thus the need for the inverse discrete Fourier transform arises. This transform is defined as

$$x_n = c_1 \sum_{j=0}^{N-1} X_j e^{i2\pi nj/N} \tag{22}$$

Where c_1 is a scaling parameter again, c_0 and c_1 are always such that $c_0 \cdot c_1 = \frac{1}{N}$. This gives the backwards approximation

$$f(x_i) \approx c_1^* x_i \tag{23}$$

The implementation for the DFT and IDFT takes care of the scaling parameters in the transforms as long as they uphold the condition

$$x_i = IDFT(DFT(x_j))_i \qquad j = 0, 1, 2, \ldots, N-1 \tag{24}$$

The implementation used in this thesis upholds this requirement, so the exact values of c_0^* and c_1^* are inconsequential. This project uses an implementation of the fast Fourier transform (FFT) and inverse fast Fourier transform (IFFT) to compute the DFT and IDFT, more precisely it uses kissfft provided by the Eigen template library for C++. With all of this in place, it is time to set up a numerical scheme to compute the time evolution of the model in equation (17). The scheme chosen is the Euler method, it is one of the less accurate methods of solving an ODE numerically, but it has the advantage of simplicity and computational efficiency. The functions in the model are discretized according to equations (18) and (19) and in time according to

$$t_j = j \cdot dt \qquad j = 0, 1, 2, \ldots \tag{25}$$

The numerical scheme to solve equation (17) by Euler's method looks like

$$\begin{aligned} H_i^j &= \text{FFT}(\mathcal{F}\{F(T_k^j)\})_i,\ k = 0, 1, 2, \ldots, N-1 \\ G_i^{j+1} &= G_i^j + dt\frac{1}{C}\left[H_i^j - (K_w k_i^2 + B)G_i^j\right] \\ T_i^{j+1} &= \text{IFFT}(\{G_k^{j+1}\})_i,\ k = 0, 1, 2, \ldots, N-1 \end{aligned} \tag{26}$$

Where G_i^j is an approximation of $G(k_i, t_j)$, $S_i = S(x_i)$, and T_i^j is an approximation of $T(x_i, t_j)$ for $j > 0$.

3.1.1 Numerical scheme

Initialize by choosing a Q, $S(x)$, $K(x)$, and $T_0(x)$, then set $T_i^0 = T_0(x_i)$ and
$G_i^0 = \text{FFT}(\{T_k^0\})_i$, $k = 0, 1, 2, \ldots, N-1$, and $S_i = S(x_i)$. Now the for step j in iteration, starting at j=0.

1. Compute the H_i^j terms by using the fast Fourier transform.
2. Compute the G_i^{j+1} values using H_i^j and G_i^j.
3. Compute the inverse fast Fourier transform of G_i^{j+1} in order to find T_i^{j+1}.
4. Add one to j and repeat step 1-3 for as many steps as required.

Because of the nature of the FFT algorithm it is also useful to choose N as a power of 2, as this takes full advantage of the optimizations of the algorithm. It is important to note that the $\mathcal{F}\{F(T)\}$ function, used in equation (26), includes some partial differential term, this term is approximated by

$$(\partial_x \hat{K} \partial_x T)_i^j \approx \frac{1}{2}(\partial_x^- \hat{K} \partial_x^+ T + \partial_x^+ \hat{K} \partial_x^- T)_i^j \tag{27}$$

Where ∂_x^+ and ∂_x^- denotes a forward and backward difference respectively. Which expands into

$$\begin{aligned} (\partial_x \hat{K} \partial_x T)_i^j \approx \frac{1}{2dx^2}(&\hat{K}_i(T_{i+1}^j - T_i^j) - \hat{K}_{i-1}(T_i^j - T_{i-1}^j) + \\ &\hat{K}_{i+1}(T_{i+1}^j - T_i^j) - \hat{K}_i(T_i^j - T_{i-1}^j)) \end{aligned} \tag{28}$$

In addition, the calculation of the partial differential terms shown here need some special care at the endpoints. The values T_{-1}^*, $\hat{K}_{-1}$, T_N and $\hat{K}_N$ are required to

compute the term on the entire discretized line. For the K-terms, they are found very simply as K can always be a constant function at the endpoints with right choice of L. Recall that it was defined as being piecewise constant. So the K-terms are

$$\begin{aligned} \hat{K}_{-1} &= \hat{K}_0 \\ \hat{K}_{N-1} &= \hat{K}_N \end{aligned} \tag{29}$$

The case is slightly more complicated for the T-terms, the way these were found was by approximating them by assuming that T has a second derivative that is near constant at the endpoints. This implies that

$$\frac{T_{-1} - 2T_0 + T_1}{dx^2} \approx \frac{T_0 - 2T_1 + T_2}{dx^2} \tag{30}$$

Which gives the approximation needed.

$$T_{-1} \approx 3T_0 - 3T_1 + T_2 \tag{31}$$

And likewise for the other endpoint

$$T_N \approx 3T_{N-1} - 3T_{N-2} + T_{N-3} \tag{32}$$

3.1.2 Stability

To run this scheme for longer periods of time it obviously has to be stable. It is known that the Von Neumann stability requirement for the PDE

$$F_t = \alpha F_{xx} \tag{33}$$

is $dt \leq \frac{1}{2\alpha} dx^2$ for the finite difference scheme [6]. The equation solved in this project is of the same base type, but it is not solved by using finite differences in this section, but rather the spectral version of the problem, although there are some terms that are approximated by finite differences methods. Thus, the same type of stability condition is assumed, $dt \leq C dx^2$. From experiments, this C was found to be approximately 1.45. Leading to the stability condition for the scheme

$$dt \leq 1.45 dx^2 \tag{34}$$

A different error comes from the $a(T)$ and $\hat{K}$ function, these functions are piecewise constant, which poses two problems. Firstly, it's impossible to discretize a piecewise constant function exactly, no matter how small dx is chosen there will be some error at the points where it's discontinuous. Another issue is that the DFT of these functions is computed to approximate their CFT, and the CFT converges very slowly to 0 when k increases for functions with discontinuities. This means that information beyond the boundaries, $-K$ and K, of the discretized domain is lost, which is undesirable. To address this, it is appropriate to introduce some smoothing to the $a(T)$ and $K(x)$ functions to make the spectral domain converge to 0 more rapidly. There are many ways to do this smoothing, for the purposes in this analysis a convolution with a gaussian function normalized to 1 on the real line is convenient.

$$f(x; s) = \frac{1}{s\sqrt{\pi}} e^{-(\frac{x}{s})^2} \tag{35}$$

Where $s > 0$ is a smoothing parameter determining the degree of smoothing. Lower values correspond to less smoothing and vice versa. Now, a piecewise constant function $g(x)$ can be smoothened by convolution with $f(x; s)$ according to

$$g^*(x) = \int_{-\infty}^{\infty} f(x - y; s) g(y) dy \tag{36}$$

where $g^*(x)$ a is a smoothened version of $g(x)$. This can be hard to do analytically for an arbitrary number of discontinuities in $g(x)$, so its discrete counterpart is used instead. This requires a discretization of $g(x)$ and $f(x; s)$. To let constant regions remain constant without any increase or decrease in value after the convolution, it is very important that the integral of $f(x; s)$ over the real line is 1. The discrete equivalent of this will be having the sum of the discretized points be 1. Because of the sharpness of $f(x; s)$ around 0 for small values of s, some extra care is required when discretizing that function as the sum of the discretized points must add up to 1. The discretization of $g(x)$ does not require this extra care. The discretization is computed by

$$\begin{aligned} g_i &= g(x_i) \\ f_j &= \int_{(j-\frac{1}{2})dx}^{(j+\frac{1}{2})dx} f(y; s) dy, \qquad j = -M, \ldots, M \end{aligned} \tag{37}$$

Where $dx = \frac{2L}{N}$ and $M = ceil(\frac{4s}{dx})$, which is large enough to make the terms add up to ≈ 1. Note that the sum won't be exactly 1, in order to fix this the f_j terms are divided by their sum after the discretization. Finally, the smoothing is computed using a discrete convolution of the discretized g_i and f_j values.

$$g_i^* = \sum_{n=-M}^{M} f_n g_{i-n} \tag{38}$$

Where g_i^* is the discretized approximation of $g^*(x)$. The main advantage of this method of smoothing is that it remains the same for any number of discontinuities in the function $g(x)$, as opposed to smoothing by using for example a hyperbolic tangent function where the complexity of the smoothing increases with number of discontinuities. However, a drawback of the convolution smoothing method is that the computational complexity is $O(M^2)$, which means that more smoothing (higher s) will be much slower than less smoothing (lower s). For the purposes in this analysis, s will be chosen to be small, as the model is parabolic and very forgiving for these rapidly changing functions.

3.1.3 Verification by artificial source

To verify that the spectral solution is correct an artificial source can be used along with a choice of $K(x)$. A choice for this is

$$\begin{aligned} T(x, t) &= \cos(x + t) \\ K(x) &= K_w \end{aligned} \tag{39}$$

Using this artificial source, the $F(T)$ function is calculated to be

$$F(T) = (B + K_w)\cos(x + t) - C\sin(x + t) \tag{40}$$

Which is enough to initialize the numerical scheme and run it for as long as desired. The result from running the

scheme for this artificial source is plotted in figure 1, comparing the numerical solution to the analytical artificial source.

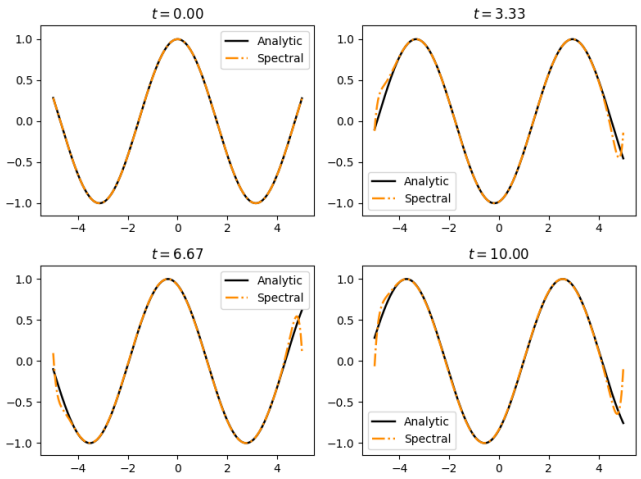

Figure 1: Comparison of analytical and numerical solution. Simulation ran with 289262 iterations. Using $N = 2048$, $L = 5$.

The plot shows that for the most part, the spectral scheme does a good job at approximating the solution. However, near the endpoints of the domain the scheme starts to deviate from the source. The reason for this is due to the periodicity that is imposed by the DFT, errors at the boundary are going to occur if the input to the transform, $F(T)$, does not satisfy this boundary conditions.

$$\begin{aligned} \mathcal{F}\{F(T)\}\Big|_{x=-L}^{x=L} &\approx 0 \\ \partial_x \mathcal{F}\{F(T)\}\Big|_{x=-L}^{x=L} &\approx 0 \end{aligned} \tag{41}$$

This artificial source gives an $F(T)$ that does very clearly not satisfy these equations, and thus the solution suffer close to the endpoints. The further away the equations are from being satisfied, the worse the error at the boundaries will get.

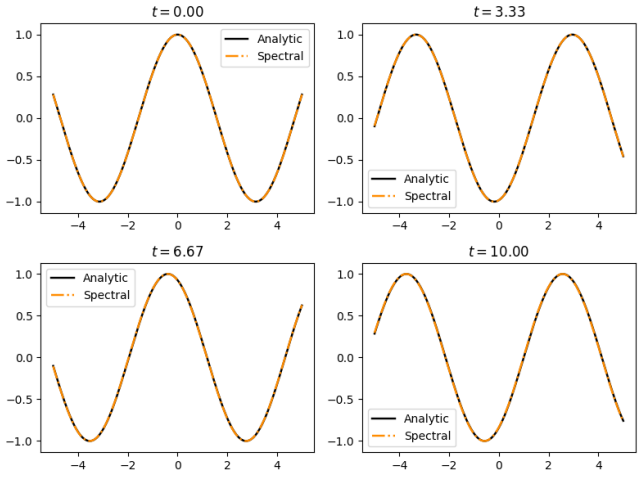

Figure 2: Comparison of analytical and numerical solution. Simulation ran with 200876 iterations. Using $N = 2048$, $L = 6$.

However, it seems that the error imposed at the boundaries dissipates rather quickly away from the edges, meaning the numerical scheme might still be useful for input that doesn't satisfy the periodicity. To find a satisfactory solution in a certain domain, one might be able to run the code on a larger domain and discard the values close to the endpoints. The same scheme was ran using $L = 6$ (figure 2), with the endpoints discarded, leaving the same range of values in as in figure 1. This numerical solution follows the artificial source very closely, highlighting that this is indeed a viable way to bypass the criteria in equation 41 when using this numerical scheme.

To further establish the method, it was also compared to the analytical solution from equation (9) for a choice of Q, $S(x)$and $T_0(x)$. Recall the analytical solution found was for the case with no continents, thus leaving $K(x) = K_w$. The choice for Q, $S(x)$ and $T_0(x)$ are

$$\begin{aligned} Q &= 340 \\ S(x) &= e^{-\frac{x^2}{10}} \\ T_0(x) &= -50 \end{aligned} \tag{42}$$

A run of the numerical scheme using the same method of discarding values close to the edges gave perfect overlap with the analytical solution. The results are shown in figure 3.

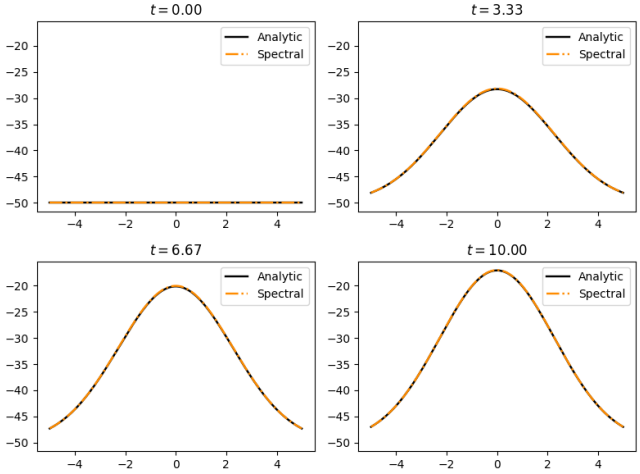

Figure 3: Comparison of analytical and numerical solution. Simulation ran with 200876 iterations of Euler's method. Using $N = 2048$, $L = 6$.

These simulations have all been computed using a constant $K(x)$ function, thus making the partial differential term in $F(T)$ equal 0. However, it must also be verified that it works when that is no longer the case. This is also done by using an artificial source. This time the choice is

$$T(x,t) = \begin{cases} -\dfrac{K_w}{K_l}(x^2 - 25), & -1 < x < 1 \\ 1 + 24\dfrac{K_w}{K_l} - x^2, & x < -1 \text{ or } x > 1 \end{cases} \tag{43}$$

and the heat diffusion function

$$K(x) = \begin{cases} K_w, & -1 < x < 1 \\ K_l, & \text{otherwise} \end{cases} \tag{44}$$

Which is the same heat diffusion function that would be used for a continent being placed at (-1,1). This particular choice of $T(x,t)$ was chosen for a reason, that reason being that the ratio between the left and right-sided

limits of the derivative of $T(x,t)$ at the discontinuities of $K(x)$, (-1 and 1), satisfies the criteria derived in appendix B. Running the spectral scheme for this choice of $T(x,t)$ and $K(x)$ gives the result shown in figure 4. Note that in this simulation a much higher value of N was used. This is due to the sharp edges of the solution at the edges of the continent. Earlier the function was smooth everywhere, which allowed for a sparser discretization.

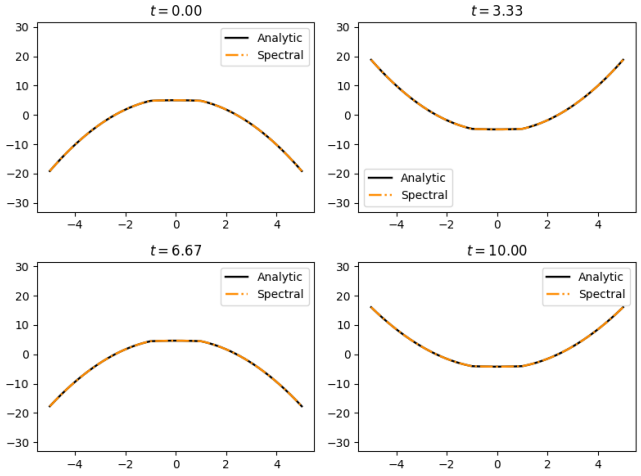

(a) Solution plotted from -5 to 5

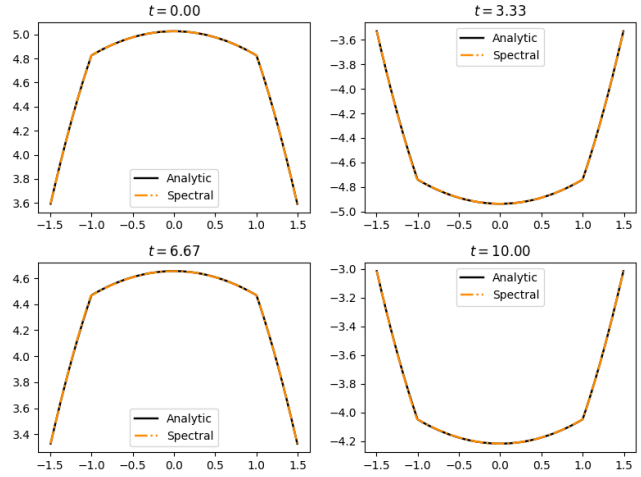

(b) Zoomed in closer to C_0 and C_1

Figure 4: Comparison of analytical and spectral solution to artificial source. Simulation ran with 803506 iterations of Euler's method. Using $N = 4096$, $L = 6$, $s = 0.005$.

As seen in the figure, the spectral scheme does an excellent job for the case with a discontinuous heat diffusion function as well. Note that the same procedure of cutting off the endpoints of the solution was used here as $F(T)$ will not satisfy the equations (41). Smoothing of the $K^*(x)$ function was also needed here, it was smoothened by the gaussian convolution described in equation (38) with smoothing parameter $s = 0.005$.

3.2 Finite differences

A second numerical scheme was devised as well, it takes the form of a finite difference scheme. This scheme solves the original model described in equation (3) instead of the spectral version of it like the spectral scheme did. The discretization of the line will be very similar to the spectral case, except that there is no need for a spectral domain, and the endpoint at L is included here. It is N equidistant points spanning the domain $[-L, L]$, and time starts at 0 and increases linearly.

$$\begin{aligned} x_i &= -L + i\frac{2L}{N-1}, & i &= 0, 1, \ldots, N-1 \\ t_j &= j \cdot dt, & j &= 0, 1, 2, \ldots \end{aligned} \tag{45}$$

Using these discretizations and the following approximations of the derivative terms in the model (104)

$$\begin{aligned} (T_t)_i^j &= \frac{T_i^{j+1} - T_i^j}{dt} \\ (\partial_x K \partial_x T)_i^j &= \frac{1}{2}(\partial_x^- K \partial_x^+ T + \partial_x^+ K \partial_x^- T)_i^j \\ &= \frac{1}{2dx^2}(K_i(T_{i+1}^j - T_i^j) - K_{i-1}(T_i^j - T_{i-1}^j) + \\ &\qquad K_{i+1}(T_{i+1}^j - T_i^j) - K_i(T_i^j - T_{i-1}^j)) \\ &= P_i^j \end{aligned} \tag{46}$$

Where $T_t(x_i, t_j) \approx (T_t)_i^j$ and $T(x_i, t_j) \approx T_i^j$. The equations show that time derivative is approximated using a forward difference. The partial differential terms are computed the same way as they were for the spectral scheme, except that here the K-function is left as is, it is not split into $K_w + \hat{K}$. This scheme will also suffer from the same end-point problems as the spectral scheme did, however, they can also be solved the same way, by using the equations (31 & 32). With this, the finite difference scheme takes form

$$T_i^{j+1} = \frac{dt}{C}\left(QS_i(1 - a(T_i^j)) - BT_i^j - A + P_i^j\right) + T_i^j \tag{47}$$

For $i = 0, 1, \ldots, N-1$, where $S_i = S(x_i)$, $a(T_i^j)$ and K_i are smoothened by the gaussian smoothing in equation (38) with smoothing parameter s. The stability criteria for this method is much more forgiving than for the spectral method, from experiments it was found to be approximately

$$dt \leq 3.48 dx^2 \tag{48}$$

Due to this, the finite difference scheme will be used for most of the subsequent stability analysis as it is both faster per iteration (mostly due to not needing to compute the FFT and IFFT), in addition to having a looser time step restriction.

3.2.1 Verification by artificial source

To verify that the scheme works it was evaluated using the same approach as earlier, an artificial source. The first choice is

$$\begin{aligned} T(x,t) &= \cos(\frac{x\pi}{10})\cos(t) \\ K(x) &= K_w \end{aligned} \tag{49}$$

The simulation result can be seen in figure 5. Which shows that the finite difference scheme can handle K being a constant function.

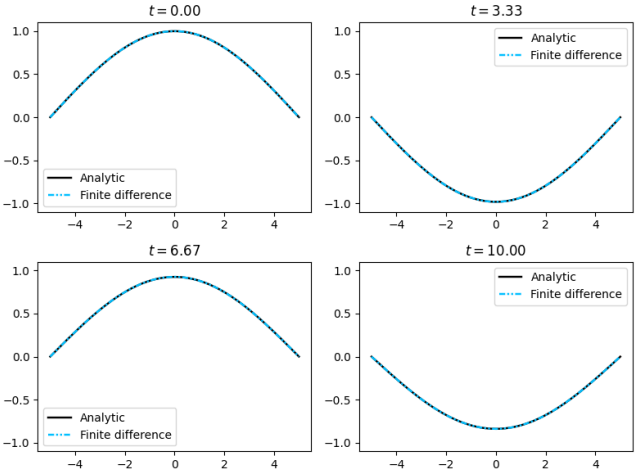

Figure 5: Comparison of analytical and numerical solution. Simulation ran with 459770 iterations. Using $N = 4001$, $L = 5$.

However, not much can be said about the case when K is no longer a constant function, which will happen when a continent is placed on the line. To test this, the same artificial source that was used to test the spectral scheme can be done. Recall

$$T(x,t) = \begin{cases} -\dfrac{K_w}{K_l}(x^2 - 25), & -1 < x < 1 \\ 1 + 24\dfrac{K_w}{K_l} - x^2, & x < -1 \text{ or } x > 1 \end{cases} \tag{50}$$

and the heat diffusion function

$$K(x) = \begin{cases} K_w, & -1 < x < 1 \\ K_l, & x < -1 \text{ or } x > 1 \end{cases} \tag{51}$$

Using this, the code was run again.

As seen in figure 6 and 7, the plots look identical to the simulations ran with the spectral code. Which shows that both numerical schemes can handle the discontinuity in the $K(x)$ function. This means that further in this thesis stationary solutions of the model in question can be tested for stability using two different numerical schemes.

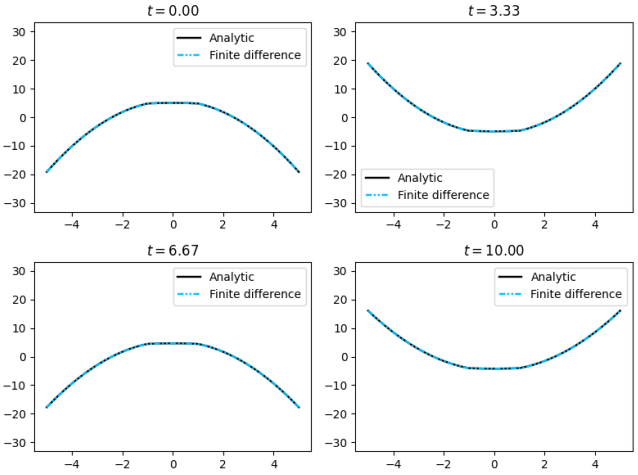

Figure 6: Comparison of analytical and finite difference solution to artificial source. Simulation ran with 459770 iterations. Using $N = 4001$, $L = 5$, $s = 0.005$.

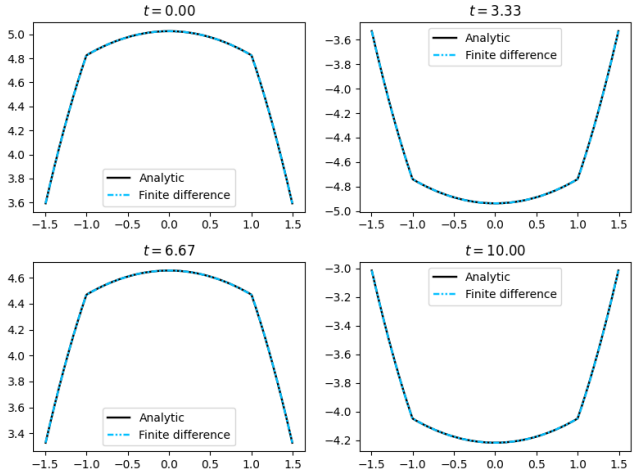

Figure 7: Figure 6 zoomed in closer to C_0 and C_1

4 Boundary formulation of stationary solutions

The next step in the analysis of the model, is to consider stationary solution. That is when the term $\partial_t T = 0$, this reduces the model to

$$-\partial_x K \partial_x T + BT = QS(1 - a(T)) - A \tag{52}$$

Let's now assume that K is constant and normalize the model according to the possible constant values of K, using the temperature scaling $T = T'T_s$. Where $-T_s = -10°C$ which is the critical sea-ice melting temperature.

$$\begin{aligned} -\partial_{xx} T' + \beta_w T' &= \eta_w S(1 - a(T')) - \alpha_w \\ -\partial_{xx} T' + \beta_l T' &= \eta_l S(1 - a(T')) - \alpha_l \end{aligned} \tag{53}$$

Where $\alpha_w = \frac{A}{K_w T_s}$, $\beta_w = \frac{B}{K_w}$, $\eta_w = \frac{Q}{K_w T_s}$ are the parameters used for the model in regions with water/ice. And $\alpha_l = \frac{A}{K_l T_s}$, $\beta_l = \frac{B}{K_l}$, $\eta_l = \frac{Q}{K_l T_s}$ are the parameters for regions with land/snow covered continent. Moving on, the subscript w denotes parameters special to water regions, and the subscript l denotes parameters special to land regions.

T' is dimensionless, and the $a(T')$ function looks slightly different.

$$a(T') = \begin{cases} a_0, & T' < -1, \text{ no continent at } x \\ a_1, & T' > -1, \text{ no continent at } x \\ a_0, & T' < 0, \text{ continent at } x \\ a_1, & T' > 0, \text{ continent at } x \end{cases} \tag{54}$$

From this point on, the prime is dropped from T' for all boundary formulations of the problem.

4.1 Greens function

This model is piecewise linear, and it can be solved using a boundary formulation of the problem. With a suitable integral identity along with a Greens function for a differential operator, stationary solutions can be found. Note: the derivation is done using the general form of the parameters, without their subscripts. The subscripts are added back later in the end of the derivation. To begin, define the differential operator for the problem, and

find an associated integral identity for the operator. The differential operator in the normalized models (53) is

$$\mathcal{L}U = U_{xx} + \beta U \tag{55}$$

The integral identity can be found by using integration by parts two times

$$\begin{aligned}\int_{x_1}^{x_2} dx\phi\mathcal{L}\psi &= \int_{x_1}^{x_2} dx\phi(-\psi_{xx} + \beta\psi) \\ &= [-\phi\psi_x]_{x_1}^{x_2} - \int_{x_1}^{x_2} dx\{-\phi_x\psi_x - \phi\beta\psi\} \\ &= [\psi_x\psi - \phi\psi_x]_{x_1}^{x_2} + \int_{x_1}^{x_2} dx\{-\phi_{xx}\psi + \psi\beta\phi\} \\ &= [\psi_x\psi - \phi\psi_x]_{x_1}^{x_2} + \int_{x_1}^{x_2} dx\psi\mathcal{L}\phi\end{aligned} \tag{56}$$

Which describes the integral identity for the operator $\mathcal{L}$

$$\int_{x_1}^{x_2} dx\phi\mathcal{L}\psi = [\psi_x\psi - \phi\psi_x]_{x_1}^{x_2} + \int_{x_1}^{x_2} dx\psi\mathcal{L}\phi \tag{57}$$

Next up is finding a Green's function for the differential operator, this is done by solving the equation

$$\mathcal{L}k(x;\xi) = \delta(x-\xi) \tag{58}$$

Where $\delta(x-\xi)$ is the Dirac delta function, which has the following properties

$$\begin{aligned}\delta(x) &= 0, \qquad x \neq 0 \\ \int_a^b dx f(x)\delta(x-y) &= \begin{cases} f(y), & \text{if } a < y < b \\ 0, & \text{otherwise} \end{cases}\end{aligned} \tag{59}$$

This makes the equation easily solvable in the two domains $x > \xi$ and $x < \xi$ because $\delta(x-\xi) = 0$ in those domains.

$$k(x;\xi) = \begin{cases} c_1 e^{\sqrt{\beta}x} + c_2 e^{-\sqrt{\beta}x} & x > \xi \\ c_3 e^{\sqrt{\beta}x} + c_4 e^{-\sqrt{\beta}x} & x < \xi \end{cases} \tag{60}$$

This equation has 4 free variables, but it has an issue of going to infinity as $x \to -\infty$ and $x \to \infty$, this would pose a problem later in the boundary formulation, as it contains an integral that goes from $-\infty$ and to ∞. However, imposing the restriction $c_1 = c_4 = 0$ will ensure that the all the integrals converge with the choices of $S(x)$ used in the thesis. Furthermore, the discontinuity at $x = \xi$ must be accounted for, this is done by integrating equation (58) on both sides around $x = \xi$.

$$\int_{\xi-\epsilon}^{\xi+\epsilon} dx\{-k_{xx}(x;\xi) + \beta k(x;\xi)\} = \int_{\xi-\epsilon}^{\xi+\epsilon} dx\delta(x-\xi) \tag{61}$$

From the properties of the δ-function, the right hand side of this equation will be equal to 1 for any $\epsilon > 0$. Now let $\epsilon \to 0$ and impose the condition that $k(x;\xi)$ is continuous, then the $\beta k(x;\xi)$ term must go to 0. Which leads to the equation

$$[-k_x(x;\xi)]_{\xi-\epsilon}^{\xi+\epsilon} = 1 \tag{62}$$

Which means that a discontinuity lies in the first derivative of $k(x;\xi)$. The two remaining constants can now be found by using this and the assumed continuity of $k(x;\xi)$

$$\begin{aligned}k_x(\xi^+;\xi) - k_x(\xi^-;\xi) &= -1 \\ k(\xi^+;\xi) &= k(\xi^-;\xi)\end{aligned} \tag{63}$$

Where ξ^+ and ξ^- denotes the limits of $x \to \xi$ from the right and left side respectively. Solving this system gives a Greens function with no free variables.

$$k(x;\xi) = \begin{cases} \frac{1}{2\sqrt{\beta}} e^{\sqrt{\beta}(\xi-x)} & x > \xi \\ \frac{1}{2\sqrt{\beta}} e^{\sqrt{\beta}(x-\xi)} & x < \xi \end{cases} \tag{64}$$

This function has the very desirable properties

$$\begin{aligned}\lim_{x\to\pm\infty} k(x;\xi) &= 0 \\ \lim_{x\to\pm\infty} k_x(x;\xi) &= 0\end{aligned} \tag{65}$$

This Greens function will be very similar for both regions with, and without a continent.

$$\begin{aligned}k_w(x;\xi) &= \frac{1}{2\sqrt{\beta_w}} \cdot \begin{cases} e^{\sqrt{\beta_w}(\xi-x)}, x > \xi \\ e^{\sqrt{\beta_w}(x-\xi)}, x < \xi \end{cases} \\ k_l(x;\xi) &= \frac{1}{2\sqrt{\beta_l}} \cdot \begin{cases} e^{\sqrt{\beta_l}(\xi-x)}, x > \xi \\ e^{\sqrt{\beta_l}(x-\xi)}, x < \xi \end{cases}\end{aligned} \tag{66}$$

Where k_w will be used in regions without a continent, and k_l will be used where there is one.

4.2 Boundary formulation using Greens function

Now it's just a matter of putting this together with the model in equation (53), the original model has a time derivative included, but in the boundary formulation only the stationary solutions are considered, so the T_t term is 0. Using the differential operator defined in (55) it is possible to rewrite the model.

$$\mathcal{L}T = \eta S(1 - a(T)) - \alpha \tag{67}$$

To find stationary solutions, use the integral identity and the Greens function from equations (57) and (64) respectively. Setting $\phi = T(x)$ and $\psi = k(x;\xi)$ gives

$$\int_{x_1}^{x_2} dx T\mathcal{L}k = \Big[\partial_x T k - T\partial_x k\Big]_{x_1}^{x_2} + \int_{x_1}^{x_2} dx k\mathcal{L}T \tag{68}$$

Using equation (58), the left hand side can be simplified to

$$\begin{aligned}\int_{x_1}^{x_2} dx T\mathcal{L}k &= \int_{x_1}^{x_2} dx T\delta(x-\xi) \\ &= T(\xi)\end{aligned} \tag{69}$$

From the definition of the Dirac delta function. The integral on the right hand side can also be simplified. Using equation (67), the integral can be written as

$$\int_{x_1}^{x_2} dx k\mathcal{L}T = \int_{x_1}^{x_2} dx k(\eta S(1 - a(T)) - \alpha) \tag{70}$$

Which gives the equation that will be used to find all the stationary solutions of the model.

$$T(\xi) = \Big[\partial_x T k - T\partial_x k\Big]_{x_1}^{x_2} + \int_{x_1}^{x_2} dx k(\eta S(1 - a(T)) - \alpha) \tag{71}$$

The entire line can now be segmented into regions where $a(T)$ in the above equation is constant within the entire region, and thus can be replaced by either a_0 or a_1. In all the cases, the parameters and Greens function are replaced with the subscript corresponding to which state the line in the region is in. There are 4 possible states the line can be in

1. Ice (using a_0 and k_w)
2. Water (using a_1 and k_w)
3. Snow (using a_0 and k_l)
4. Land (using a_1 and k_l)

Three examples of boundary formulations for different cases shows what this means in practice.

4.2.1 Ice-line without continent

For the case where the entire line is covered in ice with no continent on the line, the Greens-function will be $k_w(x;\xi)$, and the parameters will be η_w, α_w and $a(T) = a_0$. This leads to the solution for T

$$T(\xi) = \Big[\partial_x T k_w - T\partial_x k_w\Big]_{-\infty}^{\infty} + \int_{-\infty}^{\infty} dx k_w(\eta_w S(1-a_0) - \alpha_w) \quad (72)$$

In this case it is possible to simplify a lot, using the properties of the Greens function (65). It can be simplified to

$$T(\xi) = \int_{-\infty}^{\infty} dx k_w(\eta_w S(1-a_0) - \alpha_w) \quad (73)$$

Where a solution for the entire temperature profile on the line can be found by choosing a radiation distribution function $S(x)$ and a solar radiation constant Q. The only requirement is that they're chosen such that $T(\xi) < -1$ on the entire line.

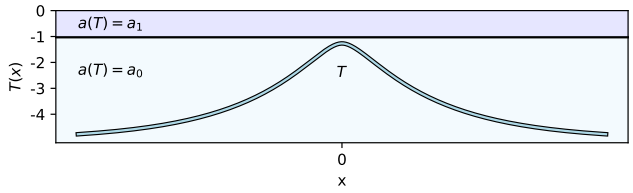

Figure 8: Example of what a solution might look in the only-ice case

In figure 8 you can see what a solution on this form might look like. The temperature profile does at no point cross the a_0/a_1 threshold, making $a(T)$ constant on the entire line. The line is coloured light blue to visualize that it is entirely covered in ice. Solutions on this form will be called "# - Ice" in bifurcation analysis, as the entire line is covered in ice.

4.2.2 Ice and water-line without continent

Another case is where the temperature $T(\xi)$ exceeds -1 in some region (A_0, A_1) surrounded by ice-regions on both sides. Then the line must be segmented into three regions, $(-\infty, A_0)$, (A_0, A_1) and (A_1, ∞). In the first region $a(T) = a_0$, in the second region $a(T) = a_1$ and in the third and final region, $a(T) = a_0$ again. Because there is no continent, the Greens function and model parameters with subscript w are used. This gives the three domains

$$\begin{aligned}
T_1(\xi) &= \Big[\partial_x T k_w - T\partial_x k_w\Big]_{-\infty}^{A_0} + \int_{-\infty}^{A_0} dx k_w(\eta_w S(1-a_0) - \alpha_w) \\
T_2(\xi) &= \Big[\partial_x T k_w - T\partial_x k_w\Big]_{A_0}^{A_1} + \int_{A_0}^{A_1} dx k_w(\eta_w S(1-a_1) - \alpha_w) \quad (74) \\
T_3(\xi) &= \Big[\partial_x T k_w - T\partial_x k_w\Big]_{A_1}^{\infty} + \int_{A_1}^{\infty} dx k_w(\eta_w S(1-a_0) - \alpha_w)
\end{aligned}$$

Where T_1, T_2 and T_3 are the temperature profiles in the first, second and third domain respectively. An issue that arises here is that the boundary values do not go to zero for the boundaries A_0 and A_1. This leaves 4 unknown quantities $T_x(A_0)$, $T_x(A_1)$, A_0 and A_1. However, certain restrictions are known. Such as, the temperature at the points A_0 and A_1 must be -1, because those are the points where the state of the line transitions from being covered in ice to being covered in water, which happens when $T(x) = -1$. This criterion must be fulfilled in all the three domains T_1, T_2 and T_3. Giving the system of equations

$$\begin{aligned}
\lim_{\xi \to A_0^-} T_1(\xi) &= -1 \\
\lim_{\xi \to A_0^+} T_2(\xi) &= -1 \\
\lim_{\xi \to A_1^-} T_2(\xi) &= -1 \\
\lim_{\xi \to A_1^+} T_3(\xi) &= -1
\end{aligned} \quad (75)$$

Which gives a determined system that can be solved. Choosing a $S(x)$ and Q will give a solution, assuming one exists for the choices made of course. The assumption for solutions on this form is that the temperature profile, $T(x)$, at some points has a region of values higher than -1, if a solution is found where this is not the case, that solution is not valid.

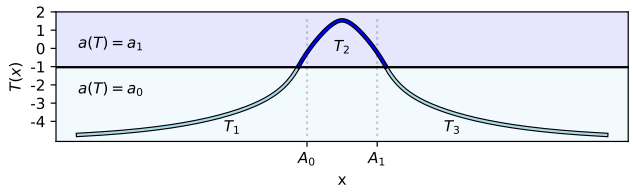

Figure 9: Example of what a solution might look like in the ice-water case

Figure 9 shows an example of what the temperature profile might look like in the case discussed here. Regions of the line covered in ice is shown as light blue again, while regions with melted water is shown in a darker blue. As you can see the temperature crosses the boundary at -1 for the region between A_0 and A_1, thus breaking the temperature profile into three regions. Each region is denoted with T_1, T_2 or T_3 depending on which equation determines the temperature profile in the region. Solutions on this form will be called "# - IceWaterIce" in bifurcation analysis, as the line, from the left, is first covered in ice, then transitions to water, then back to ice.

4.2.3 Ice covered line with continent

The last case to show how the boundary formulations are made, is the case where the line consists of only ice with a continent placed on the centre of the line from $(-1, 1)$ containing only snow. This time it is also necessary to split the line into three regions, $(-\infty, -1)$, $(-1, 1)$ and $(1, \infty)$. Where the first and third region will use the

model parameters with the subscript w, and the middle region will use the ones subscripts l. Giving the equations

$$\begin{aligned} T_1(\xi) &= \Big[\partial_x T k_w - T\partial_x k_w\Big]_{-\infty}^{-1} + \int_{-\infty}^{-1} dx k_w(\eta_w S(1-a_0) - \alpha_w) \\ T_2(\xi) &= \Big[\partial_x T k_l - T\partial_x k_l\Big]_{-1}^{1} + \int_{-1}^{1} dx k_l(\eta_l S(1-a_0) - \alpha_l) \\ T_3(\xi) &= \Big[\partial_x T k_w - T\partial_x k_w\Big]_{1}^{\infty} + \int_{1}^{\infty} dx k_w(\eta_w S(1-a_0) - \alpha_w) \end{aligned} \tag{76}$$

There are 4 unknown quantities in these equations, $T(-1)$, $T(1)$, $\partial_x T(-1)$ and $\partial_x T(1)$. This time around, the temperatures at the endpoints of the continent are unknown, so other restrictions are needed to determine the system. The first two comes from the continuity of the temperature profile, and the last two comes from the particular discontinuity in the derivative of T across the water-continent edge. Giving

$$\begin{aligned} \lim_{\xi\to -1^-} T_1(\xi) &= \lim_{\xi\to -1^+} T_2(\xi) \\ \lim_{\xi\to 1^-} T_2(\xi) &= \lim_{\xi\to 1^+} T_3(\xi) \\ \lim_{\xi\to -1^-} K_w\partial_x T_1(\xi) &= \lim_{\xi\to -1^+} K_l\partial_x T_2(\xi) \\ \lim_{\xi\to 1^-} K_l\partial_x T_2(\xi) &= \lim_{\xi\to 1^+} K_w\partial_x T_3(\xi) \end{aligned} \tag{77}$$

A more detailed derivation of the boundary condition for the derivative terms can be found in appendix B. With this the system is determined and a solution for the temperature profile may be found by choosing a $S(x)$ and Q, if one exists. The assumption here is that $T_1 > -1$ and $T_3 < -1$ in their respective domains, and that $T_2(\xi) < 0$ within its domain. Any solution on this form breaking these criteria is not a valid solution.

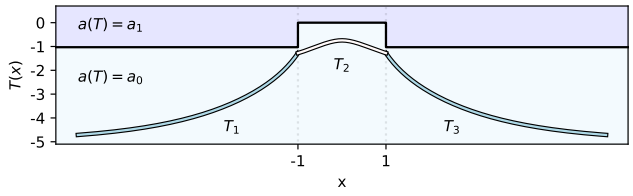

Figure 10: Example of what a solution might look like in the ice-snow case wit a continent

In figure 10 you can see an example. Regions of the line with ice is light blue again, and regions with a snow covered continent is presented in white. A difference between this boundary formulation and the previous two is more clearly displayed here, the change from using $a(T) = a_0$ to $a(T) = a_1$ is no longer a simple constant threshold. This example has $T(\xi) > -1$ for a small region inside (-1, 1), but in this region the threshold is changed, thus the albedo is a_0 on the entire line. You can also see what the discontinuous derivatives at the endpoints of the continent look like. Solutions on this form will be called "# - IceSnowIce" in bifurcation analysis, as the line, from the left, is first covered in ice, then snow covered continent, and last back to ice again. All solutions will be named according to what state the line is in from left to right in this fashion.

5 Bifurcation analysis

Now that a method of finding stationary solutions to the model have been found, it is possible to draw bifurcation diagrams for the model. All that is required is to choose a function $S(x)$, and solve the boundary formulations while letting Q vary. This was done for several different cases, without a continent, with a symmetrically placed continent, with a non-symmetrically placed continent, and for two different choices of $S(x)$. In this project they will be chosen to have the same shape as probability density functions. All solutions will also be tested for stability numerically by adding a small perturbation to each solution and computing the time evolution using the finite difference scheme with parameters

$$\begin{aligned} N &= 4001 \\ L &= 6 \\ s &= 0.001 \\ T_0 &= T(x_i) + \epsilon \end{aligned} \tag{78}$$

and ran until $t = 50$ (1 596 424 iterations). The time evolutions are then compared to the unperturbed stationary solution at each point and given an error value by the sum of their square differences

$$E = \sum_{i=0}^{N-1} dx(T_i^* - T(x_i))^2 \tag{79}$$

Where T_i^* is the time evolution from the finite difference scheme at $t = 50$, and $T(x_i)$ is the discretized stationary solutions. This stability analysis is done for an upward perturbation $\epsilon = 0.01$, and a downward perturbation $\epsilon = -0.01$. This analysis has a few drawbacks, it is unable to completely determine if a solution is stable or not. Some solutions might go unstable here that in the analytical case might not really be unstable, and vice versa, it can however give some insight into the stability of solutions. In addition, the numerical scheme must be stopped at some point, which means that solutions that goes unstable very slowly might be overlooked. Lastly, the numerical schemes are unable to compute the stability on the infinite line, however, the behaviour of the solutions outside the domain (-L,L) is just exponential decay toward the limiting value $-\frac{A}{B} = -49.92$, so it is unlikely that this has a very big impact. It is also important to note that the boundary formulations and the numerical schemes use different temperature scalings, this must be taken into account before running the simulations.

5.1 No continent

Starting with the simplest case, having no continent on the line. In this case the heat diffusion function is constant, $K = k_w$. So each point x_0 of the line can be in only one of two states, either it is covered in ice $a(T(x_0)) = a_0$, or it is covered in water $a(T(x_0)) = a_1$. This is the same case that was considered by North, except his analysis was on a half sphere rather than the infinite line.

5.1.1 Laplacian $S(x)$

With the choice of a Laplacian-type $S(x)$

$$S(x) = e^{-\frac{|x|}{2}} (= 4\text{Laplace}(0, 2)) \tag{80}$$

The bifurcation diagram was computed, and it is shown in figure 11 along with the stability plots.

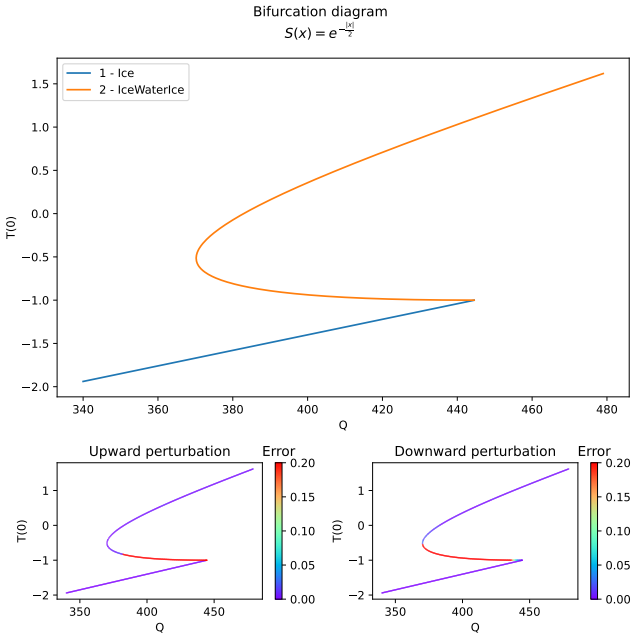

Figure 11: Bifurcation diagram for symmetric exponential $S(x)$ (Using boundary formulations C.1, C.2)

The result is similar to what North found in 1975. The model has a bistability with an unstable region connecting the two stable ones. However, it seems that the instability is most prominent for the downward perturbation, for the upward perturbation the solution is numerically stable in a larger region and the downward perturbation. Another thing to note is that in the downward perturbation, the region where the solutions transition from being stable to unstable (around Q=440), there looks to be a smooth transition. This is only due to the fact the time evolution converges to the stable solution from "1 - Ice" for the same Q, and in this area the solutions are very close to each other. In fact, for every solution marked in red for the downward perturbation, the time evolution converges to the stable solution in "1 - Ice"

5.1.2 Gaussian $S(x)$

With the choice of a Gaussian-type $S(x)$

$$S(x) = \frac{4}{\sqrt{10\pi}} e^{-\frac{x^2}{10}} (= 4N(0, 10)) \tag{81}$$

The bifurcation diagram in this case, in figure 12 looks very similar, it has a very similar shape, similar bistability, and a similar region of stable and unstable solutions.

The stable region of solutions looks to be almost identical to the Laplacian case, the most substantial difference between the two are the values of Q in which the bistability lies in. For the Laplacian case, the bistability lies in the range $Q \in (370.21,\ 444.62)$, but for the Gaussian case it lies in the range $Q \in (441.51,\ 548.68)$. The reason for the increase in Q between the two choices of $S(x)$ is because the Gaussian-type is much "wider" than the Laplacian-type, meaning that the radiation input on the line is more evenly spread out. This causes the Gaussian case to require a higher value of Q than the Laplacian case does to reach the same temperature at $T(0)$.

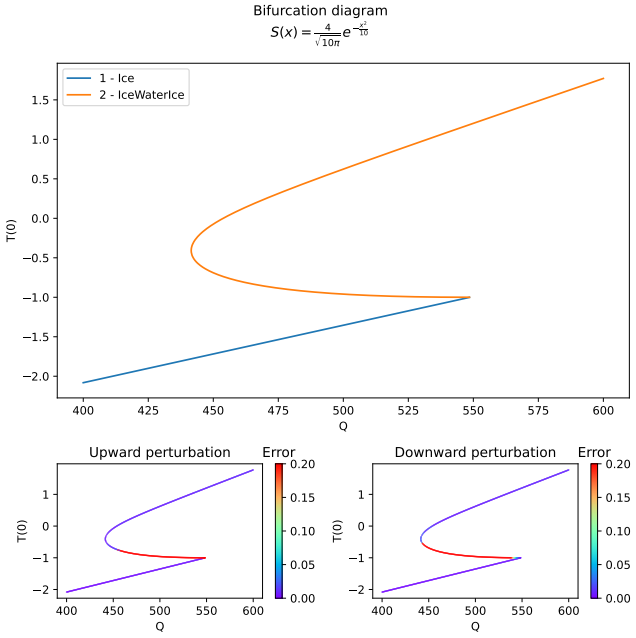

Figure 12: Bifurcation diagram for gaussian $S(x)$ (Using boundary formulations C.1, C.2)

An illustration of this is shown in figure 13, the ice only solution from both cases are plotted. This clearly illustrates that the solutions from the Gaussian-type $S(x)$ have its energy more evenly distributed that the Laplacian-type does. And thus requires a higher value of Q to reach the same temperatures at the centre of the continent compared to the Laplacian.

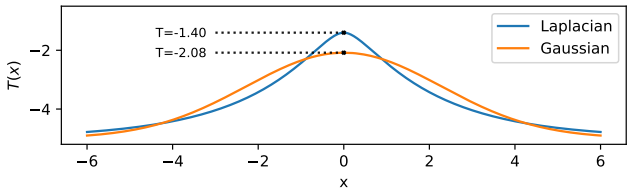

Figure 13: Temperature profiles for Q=400 for both the Laplacian and the Gaussian choices of $S(x)$

The bistability found for these two choices of $S(x)$ are both very similar to what North found, the case where the entire line is covered in ice has a unique solution everywhere a solution exists. While the case where there are two ice-edges on the line, there is a region with two solutions, where one of them is unstable.

5.2 Symmetric continent

Up to this point, the results are very much a reiteration of what North has already found. However, by placing a continent on the line at (-1, 1), the heat diffusion function is no longer constant. Making this new and unexplored territory. The choice of continent placement makes the heat diffusion function

$$K(x) = \begin{cases} K_l, & -1 < x < 1 \\ K_w, & \text{otherwise} \end{cases} \tag{82}$$

5.2.1 Laplacian $S(x)$

The same Laplacian-type $S(x)$ function from the last section was used in this case to compute the bifurcation diagram as well.

$$S(x) = e^{-\frac{|x|}{2}} (= 4\text{Laplace}(0, 2)) \tag{83}$$

This time the diagrams look a bit different, seen in figure 14. There is still a bistability, but the region of instability now covers three entire family of solutions, not a subset of one of the families as it were for the cases without a continent.

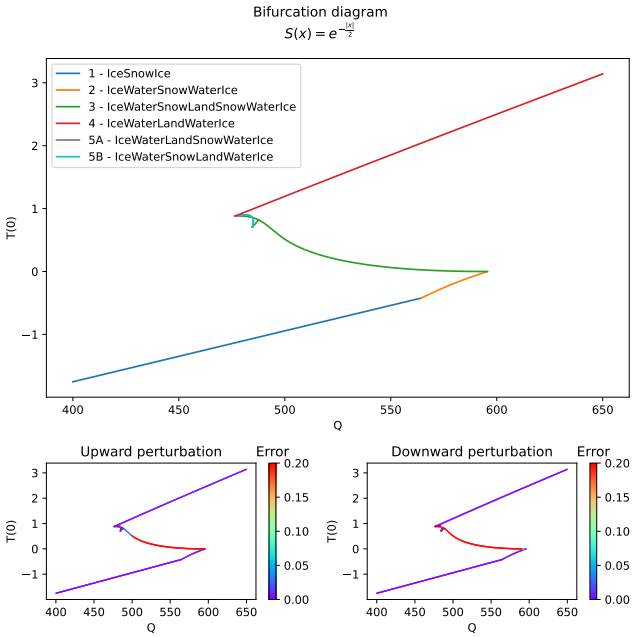

Figure 14: Bifurcation diagram for Laplacian $S(x)$ with a continent (Using boundary formulations C.3, C.4, C.5, C.6, C.9, C.10)

In the figure the solution families 4, 5A, and 5B are all unstable. Important to note that the solutions 5A and 5B are completely overlapping in the figure, so only family 5B is visible in the plot. Solutions in the families 5A and 5B are unsymmetrical around 0, but correlate to each other by $T_{5A}(x) = T_{5B}(-x)$ and vice versa for the same value of Q. In quantum mechanics this is called a parity inversion, it is shown in figure 15.

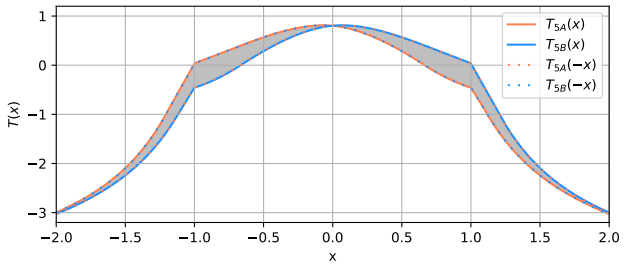

Figure 15: Solutions 5A and 5B and their inversions plotted for Q=485.15

These solutions begin at the same point where family 6 and 4 start, but follow a path in between the two families, before it begins to curve downward and transition to solutions contained in family 4, which then traces a straight line back to its main path of solutions. This straight line tracing the path between the main family-4-path and the end of family 5A and 5B, contain two different overlapping asymmetrical solutions. These two solutions are also parity inversion of each other. The two solutions grow less asymmetrical and increasingly similar, while still maintaining they parity inversion, as they get closer to the main family 4 line. Figure 16 shows a better illustration of what happens.

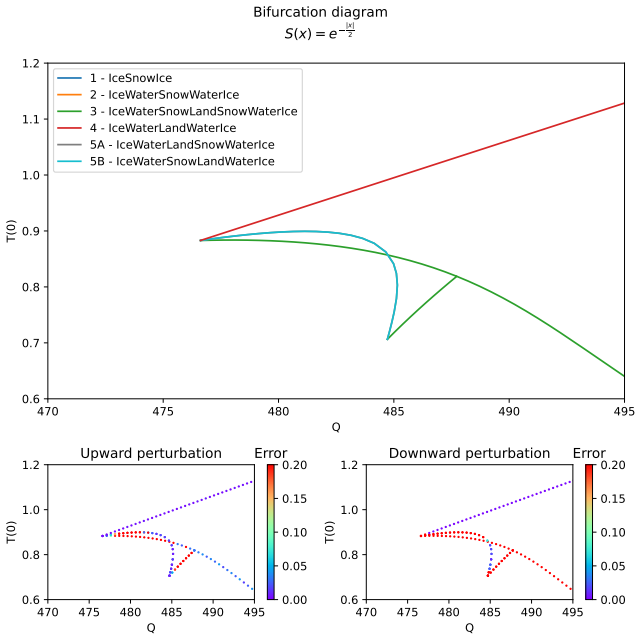

Figure 16: Bifurcation diagram from figure 14 zoomed in near the unsymmetrical solutions

The numerical stability of these solutions also contain intricate behaviour, it seems that some of the unsymmetrical solutions are stable for small perturbations. They appear to be more able to handle upward perturbations than they are downward perturbation. Similar to what was found in the case without a continent where a larger number of solutions were numerically stable for upward perturbations. This might be due to the limitations of the stability test as mentioned earlier. The reason for these values is because of the limitation on the length of the simulations. They are ran up to $t = 50$, this is able to catch a lot of the unstable solutions, but some of them go unstable slowly enough to not exceed a total square error 0.2. A region of the solutions in family 4 has errors in the range 0.05 to 0.10, between $Q \approx 485$ and $Q \approx 500$, for the upward perturbation. These solutions are in the process of going unstable, but the simulation was stopped too early to completely catch their instability.

5.2.2 Gaussian $S(x)$

The Gaussian-type radiation distribution is a bit different in this case than it was for the case without a continent. Here the following distribution is used instead.

$$S(x) = \frac{4}{\sqrt{5\pi}} e^{-\frac{x^2}{5}} \tag{84}$$

There is a good reason for this change, recall in the last section the gaussian-type used had a standard deviation of 10, while here it is 5, meaning that the distribution is

more focused around $x = 0$ here than it previously was. The bifurcation diagram for this choice of $S(x)$ is shown in figure 17. Continent is still placed at (-1, 1).

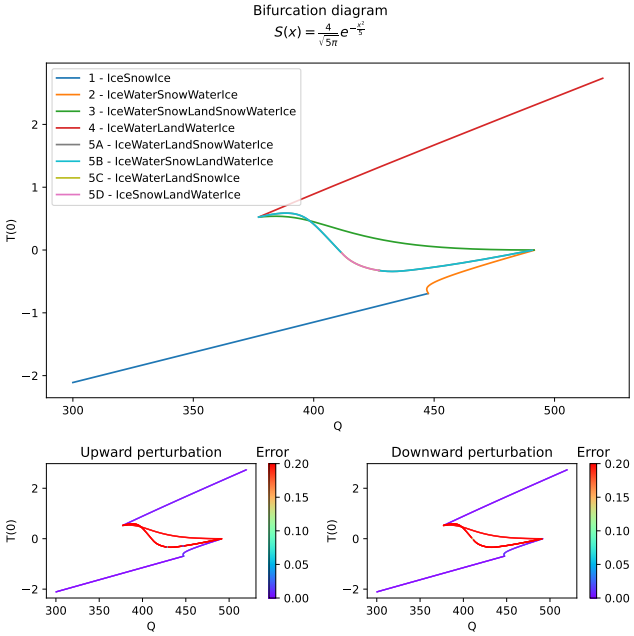

Figure 17: Bifurcation diagram for Gaussian $S(x)$ with a continent (Using boundary formulations C.3, C.4, C.5, C.6, C.9, C.10, C.11, C.12)

This bifurcation diagram has even more unsymmetrical solutions than the Laplacian had, every solution in the families 5A, 5B, 5C and 5D are unsymmetrical. Families 5A and 5B are completely overlapping and parity inversions of each other, the same goes for 5C and 5D. The interesting part here is that the unsymmetrical solutions trace a complete alternative path between family 2 and 4 rather than converging back to family 3 like the Laplacian case did. Family 2 also differs from what was found in the Laplacian case, here it begins going left before it curves to the right and continues straight until it meets families 4, 5A and 5B. Meaning that for some small region of Q there are two different solutions for family 2. This is a miniature version of the case without a continent, where the ice edges can be in two distinct positions and still be a stationary solution for the same Q. It is suspected that it is the "width" of the Gaussian $S(x)$ allows this to happen, while the Laplacian case is too "narrow". The stability of the solutions in this case are much less complex, the solutions in families 1, 2 and 4 are stable, while the rest are unstable.

Further, by allowing the Gaussian type $S(x)$ to be even wider, the behaviour mentioned earlier of family 2 should be even more similar to the case without a continent. Using

$$S(x) = \frac{4}{\sqrt{6\pi}} e^{-\frac{x^2}{6}} \tag{85}$$

And computing the bifurcation diagram in figure 18, the continent is still placed at (-1, 1). The leftward path of family 2 before curving right is substantially longer than it was in the slightly narrower Gaussian. Leading to a tristability in a small region, this region could be made larger by shrinking the size of the continent or making $S(x)$ even wider. However, this is hardly the most noteworthy difference. That would be the introduction of families 3A and 3B. These solution families are considerably different from any of the solution families in the previous bifurcation diagrams.

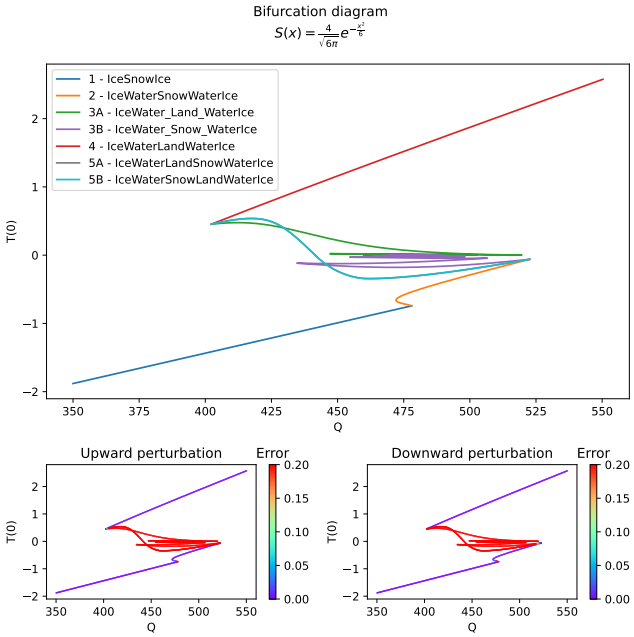

Figure 18: Bifurcation diagram for Gaussian $S(x)$ with a continent (Using boundary formulations C.3, C.4, C.6, C.9, C.10, C.13)

It's important to note that the solutions 3A and 3B are special and contain multiple subfamilies. All symmetric boundary formulations with more than 2 snow-land/land-snow transitions on the continent are contained in these two families (see 2-N boundary formulations in appendix C.13). 3A contain the families that has land at the centre of the continent, and 3B contain all families where the centre is covered in snow instead. Every time the line does a 180 direction change in 3A and 3B corresponds to the solution having an additional two snow-land transitions. In this bifurcation diagram, only solutions with up to 40 transitions were computed, but there seems to be no upper bound to the number of transitions possible. While computing the solutions, it was noted that the derivative on all transitions, $T_x(B_i)$ in the formulations, on the continent get smaller and smaller with more snow-land transitions on the continent. The temperature at $x = -1, 1$ also go closer and closer to 0 as the number of transitions increases. If this pattern continues for both the boundary temperature and transition derivatives, as the number of transitions go to infinity, it would be possible to find an exact solution to what the temperature profile would look like in the limiting case. There is no longer any need to model what happens over the continent as the temperature would just be 0 across all of it (because $T_x(B_i) \to 0$ and $T(B_i) = 0$), the only regions that need to be modelled, are what happens to the right and left side of the continent. In addition, because the solution is symmetric nothing is lost by only modelling the right side of the continent, and then just mirroring the result around 0. The equations to model

this will be

$$
\begin{aligned}
T_1(\xi) &= 0 \\
T_2(\xi) &= \Big[\partial_x T k_w - T\partial_x k_w\Big]_1^{A_0} + \int_1^{A_0} dx k_w(\eta_w S(1-a_1) - \alpha_w) \\
T_3(\xi) &= \Big[\partial_x T k_w - T\partial_x k_w\Big]_{A_0}^{\infty} + \int_{A_0}^{\infty} dx k_w(\eta_w S(1-a_0) - \alpha_w)
\end{aligned} \tag{86}
$$

Where T_1 is the continent from (0, 1), and T_2 models (1, A_0) and T_3 model (A_0, ∞). A_0 is the position of the ice-water transition to the right of the continent. The unknown quantities here are A_0, $T'(A_0)$ and the Q that supports a solution on this form. In this case there are more restrictions than there are unknown quantities. The restrictions are

$$
\begin{aligned}
\lim_{\xi\to 1^+} T_2(\xi) &= 0 \\
\lim_{\xi\to 1^+} T_2'(\xi) &= 0 \\
\lim_{\xi\to A_0^-} T_2(\xi) &= -1 \\
\lim_{\xi\to A_0^+} T_3(\xi) &= -1
\end{aligned} \tag{87}
$$

All these equations must be fulfilled in order for the solutions to be valid. This is an over-determined system, but it does still have a solution, plotted in figure 19. And it gives $Q \approx 479.633$, this matches with what was found in the bifurcation diagram. From figure 18 it looks as if the solution families 3A and 3B converge to each other at around $Q \approx 480$, which is consistent with what was found in the theoretical limiting case. For the stability, similar to the narrower Gaussian, only solutions in the families 1 and 4 are stable. Solution 2 has similar stability to the "# IceWaterIce" solutions in the case without a continent, there are some unstable solutions directly connected to the first solution family with stable solutions directly above in the diagram. By either making $S(x)$ wider, or the continent smaller, the similarity could be more apparent, but this thesis will not do that. The rest of the families are all unstable, for both negative and positive perturbations.

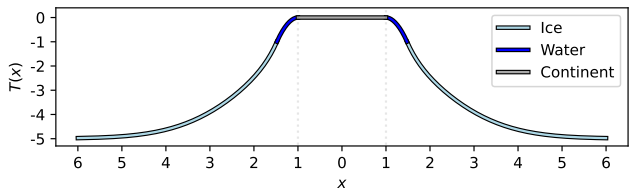

Figure 19: Plot of how the theoretical limiting case would look

The reason all the solution families 3A and 3B appear only for this choice of $S(x)$, and none of the earlier ones, is due to the way solution family 2 break. Figure 20 shows the different ways solution family 2 breaks down in the two cases. This family assumes that the entire continent is covered in snow, this assumption breaks when temperature on the continent passes 0 at any point. In the Laplacian case, this assumption is broken by the temperature at the centre of the continent reaching 0.

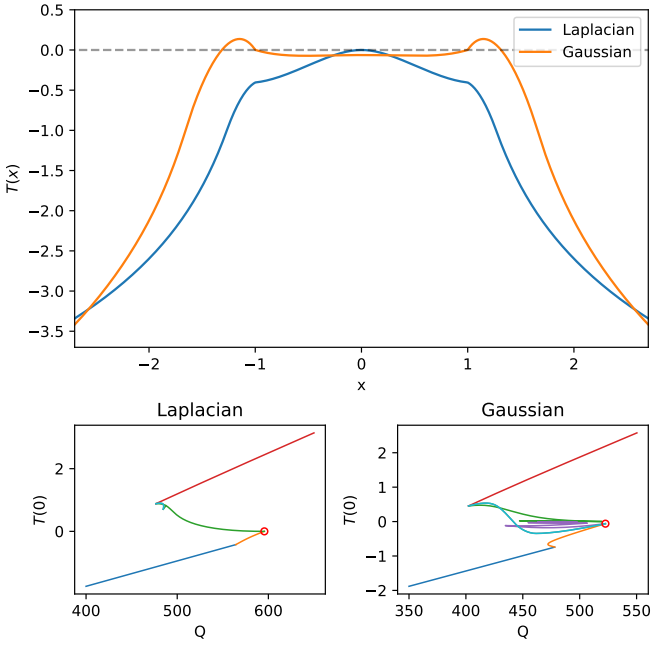

Figure 20: How solution family 2 breaks for the Laplacian (figure 14) and the wide Gaussian (figure 18). Red circles show where the solution plotted is located in their respective bifurcation diagrams

While in the Gaussian case it is broken by the continental edges temperatures reaching 0 instead, which is what initiates all the solutions in family 3B and conversely 3A. Even though the Gaussian $S(x)$ has its maximum at $x = 0$, the continent has a higher heat diffusion parameter than the regions with water on each side. Causing energy to be transferred away from the continent at a high enough rate to allow it to build up in the water on each side of the continent, which in turn warms up the continental edges, making the edges have the highest temperature on the continent (Gaussian in the figure 20). When $S(x)$ is narrower, the higher heat diffusion parameter of the continent is not enough to make the edges warmer than the centre (Laplacian in the figure 20), which is why the families 3A and 3B does not appear in any of the other bifurcation diagrams. They would also not exist at all if the heat diffusion parameter was lower for the continent that it was for the water regions, no matter how wide $S(x)$ was made.

5.3 Unsymmetrical continent

In all of the previous computations the continent had been placed down on the centre of the line, such that it is symmetric around 0 along with $S(x)$. This gave mostly symmetrical solutions, and all cases had a form of bistability. If the continent was placed asymmetrically, it is of interest to see what happens with the bistability of the model. The continent was moved to $(-1+\epsilon, 1+\epsilon)$, for some choices of $\epsilon > 0$. The choice of radiation distribution is the same Laplacian-type as in the previous section.

$$
S(x) = e^{-\frac{|x|}{2}} \tag{88}
$$

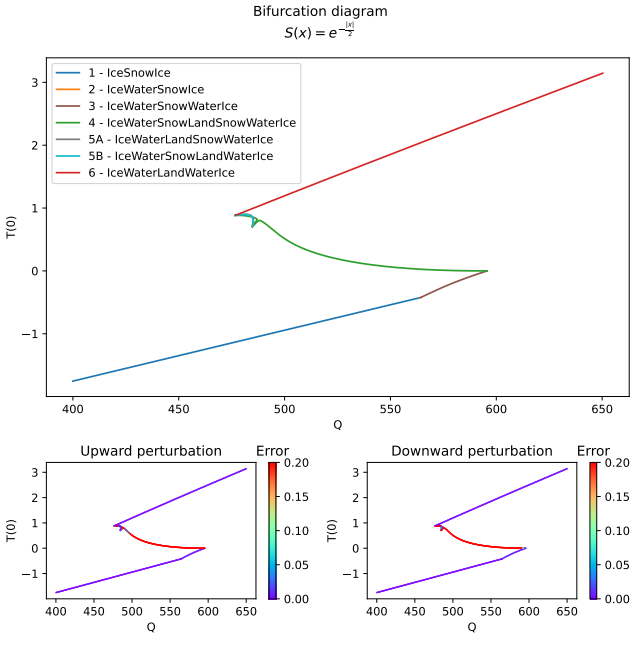

Figure 21: Bifurcation diagram for Laplacian $S(x)$ with a continent offset by $\epsilon = 0.001$ (Using boundary formulations C.3, C.7, C.4, C.5, C.6, C.9, C.10)

In figure 21 the bifurcation diagram was drawn for an offset of $\epsilon = 0.001$. This diagram looks very similar to the one without an offset in figure 14, except that this time the asymmetric solution family 5A does not perfectly overlap with 5B. There is also an additional solution family here, 2, that is in between 1 and 3. It covers such a small region that it is difficult to see in the figure, but rest assured, it is there. The most interesting thing that happens here, is that the solution family 5B, along with a subset of solutions from 4, form a loop of solutions that are not connected to any of the other solutions in the diagram. All the earlier bifurcation diagrams had every solution family have been connected to a "main path", when the continent has been moved, this is no longer the case.

The numerical stability of the solutions is also very similar to the case without the offset of the continent, solution family 1, 2, 3 and 6 seem to be stable, and a small subset of family 5A and 5B looks to be stable. But again, this might just be due to the limitation of the stability test. The bifurcation diagrams for offsets $\epsilon = 0.003$ (figure 22), $\epsilon = 0.005$ (figure 23), $\epsilon = 0.010$ (figure 24) and $\epsilon = 0.015$ (figure 25) all look very similar. They show that when ϵ increases, the unconnected solution loop made up by 4 and 5B stray further and further away from the fully connected solutions, as well as the loop shrinks in size. Solution family 2 and 5A also grow in size making family 4 and 6 stray apart, otherwise not much happens until the displacement of the continent reach $\epsilon = 0.020$. This is where the unconnected solution loop stops existing. Upon closer inspection, it was found that they disappear when the offset reach $\epsilon \approx 0.016037$. The bifurcation in for offsets $\epsilon = 0.020$ and $\epsilon = 0.030$, in figures 26 and 27 respectively, are almost identical. The solution families 2 and 5A grow a little in size, further increasing the distance between family 4 and 6, but the main shape and numerical stability is largely the same. When the offset reaches $\epsilon = 0.040$ something new happens, the introduction of two new boundary formulations, family 4B and 5C. These increase in size when the offset is further increased to $\epsilon = 0.050$, and if more bifurcation diagrams were computed these solutions would start to replace many of the symmetrically named boundary formulations. The stability here is still similar to the stability for the previous offsets. With more offset, family 5A covers a larger portion of the bifurcation diagram, and it seems that many of the solutions within that family are stable for both upward and downward perturbations. It is difficult to say if these solutions are in fact analytically stable or not, but if they eventually go unstable they take a long time to do so.

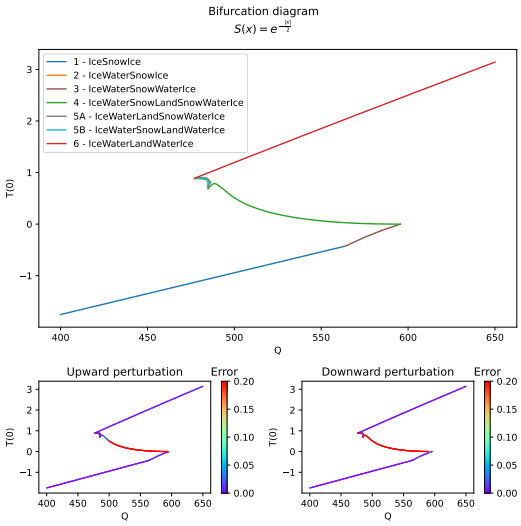

Figure 22: Bifurcation diagram for Laplacian $S(x)$ with a continent offset by $\epsilon = 0.003$ (Using boundary formulations C.3, C.7, C.4, C.5, C.6, C.9, C.10)

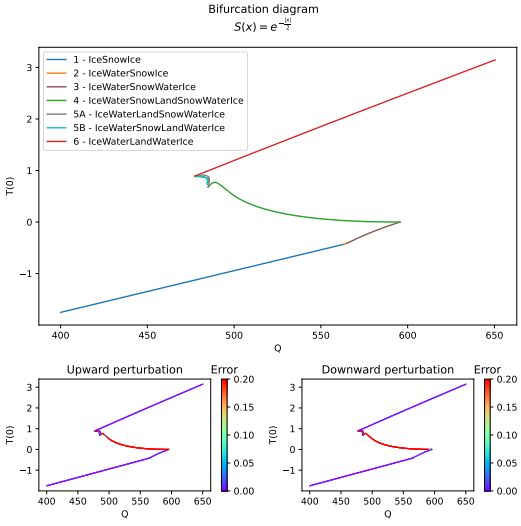

Figure 23: Bifurcation diagram for Laplacian $S(x)$ with a continent offset by $\epsilon = 0.005$ (Using boundary formulations C.3, C.7, C.4, C.5, C.6, C.9, C.10)

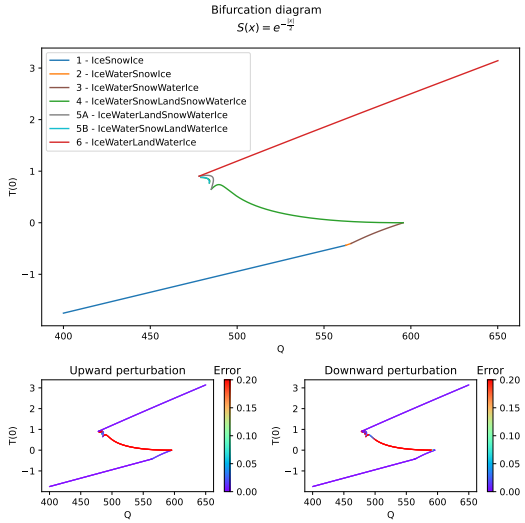

Figure 24: Bifurcation diagram for Laplacian $S(x)$ with a continent offset by $\epsilon = 0.010$ (Using boundary formulations C.3, C.7, C.4, C.5, C.6, C.9, C.10)

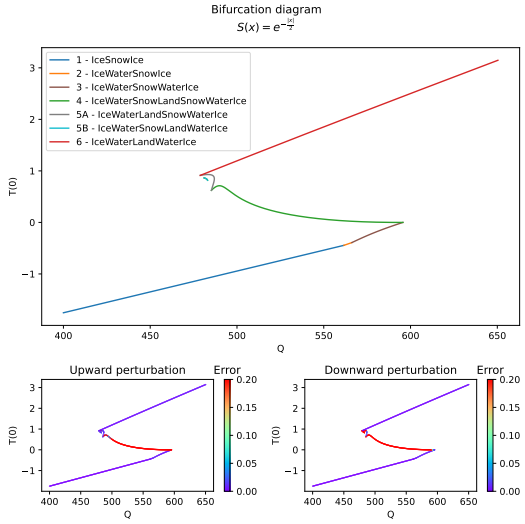

Figure 25: Bifurcation diagram for Laplacian $S(x)$ with a continent offset by $\epsilon = 0.015$ (Using boundary formulations C.3, C.7, C.4, C.5, C.6, C.9, C.10)

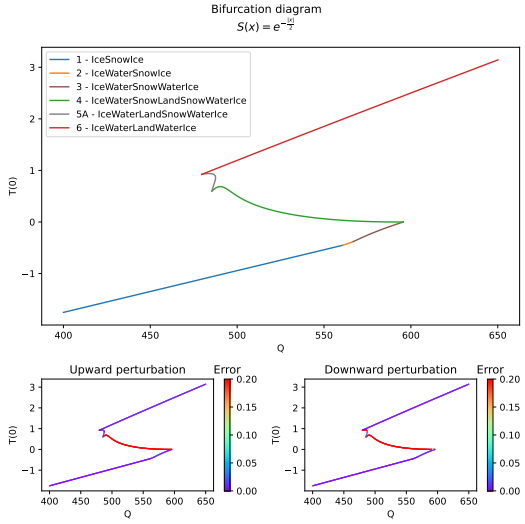

Figure 26: Bifurcation diagram for Laplacian $S(x)$ with a continent offset by $\epsilon = 0.020$ (Using boundary formulations C.3, C.7, C.4, C.5, C.6, C.9)

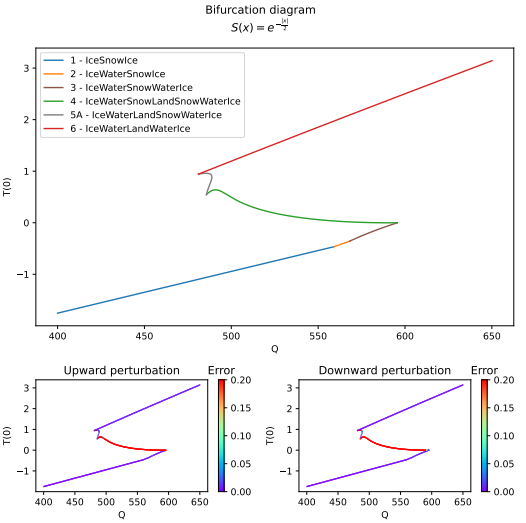

Figure 27: Bifurcation diagram for Laplacian $S(x)$ with a continent offset by $\epsilon = 0.030$ (Using boundary formulations C.3, C.7, C.4, C.5, C.6, C.9)

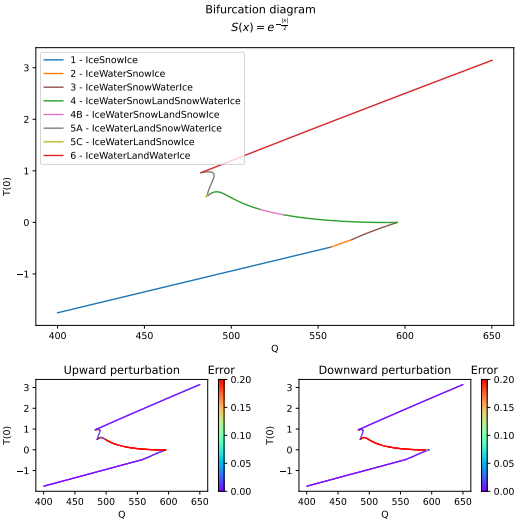

Figure 28: Bifurcation diagram for Laplacian $S(x)$ with a continent offset by $\epsilon = 0.040$ (Using boundary formulations C.3, C.7, C.4, C.5, C.6, C.8, C.9, C.11)

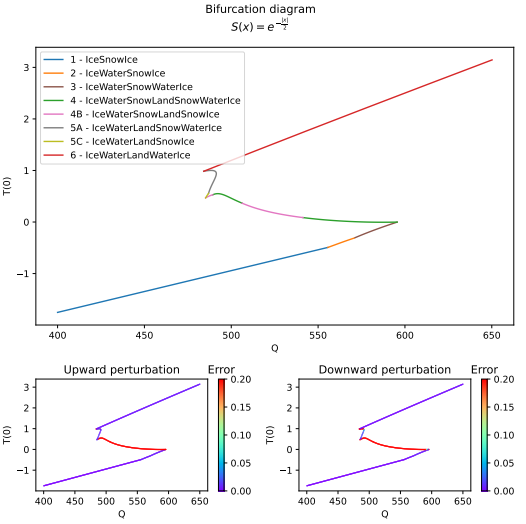

Figure 29: Bifurcation diagram for Laplacian $S(x)$ with a continent offset by $\epsilon = 0.050$ (Using boundary formulations C.3, C.7, C.4, C.5, C.6, C.8, C.9, C.11)

6 Conclusion

For the case without a continent on the line, much of North's work was recreated. The bifurcation diagrams in figure 11 and 12 shows a bistability, with an unstable solution in between the stable ones. The most notable difference between the two choices of radiation distribution functions S(x), were for which values of Q the bistability took place. With the Laplacian case having lower values of Q than the Gaussian case. In the case where a continent was placed at the centre of the line, from -1 to 1, much more complicated behaviour was found. There was still a bistability for the most part, but a different form of bistability. For the Laplacian radiation distribution function, in figure 14, the bistability differs from the one found in the case without a continent in that it is no longer due to having two distinct position of ice-water edges for the same Q. Another important distinction is that unsymmetrical solutions were found. In the case where the continent was placed on the centre of the line, the unsymmetrical solutions always came in pairs that were parity inversion of one another, and they made the bifurcation diagram connected. When the continent was moved to the right (figures 21, 22, 23, 24, 25, 26, 27, 28, 29), the resulting bifurcation diagrams became unconnected, where an unconnected loop of solutions (family 5B and a subset of family 4) appeared. This loop was most prominent when the continent was closest to the centre, and shrunk in size when it was moved further and further away before it disappeared at around the offset $= 0.016037$. A small subset of the unsymmetrical solutions also seemed to be stable in the numerical stability test performed on the solutions, leading to a possible tristability in a small region. For the Gaussian radiation distribution function for the case with a continent (figure 17), the unsymmetrical solutions traced the entire path between solution families 4 and 2 in the bifurcation diagram, rather than making a smaller loop as in the Laplacian case. They were still parity inversion of each other, but this time around none of the solutions seemed to be stable. A slightly "wider" Gaussian (figure 18) gave the same alternative path between families 4 and 2 with unsymmetrical solutions that were parity inversion of each other. However, this time the symmetrical path between 4 and 2, if there is one, contained an infinite number of solutions families. The special families 3A and 3B, each containing multiple families, seem to converge toward each other, and a heuristic limiting case was derived that included a uniform 0-degree temperature across the entire continent. For the wider Gaussian a similar type of bistability as in the case without a continent was found by looking at families 1 and 2 in the bifurcation diagram. This bistability was also caused by having solutions for two different positions of the ice-water edges for the same Q, exactly as in the case without a continent. Thus, a tristability for a small region of Q values exists for this case, this tristability is more certain than the one for the Laplacian case as it is due to the same phenomenon that happened in the case without a continent, where the bistability has been proven by North. This phenomenon can be made more apparent in the case with a continent by either making the radiation distribution function wider or making the continent smaller.

Further research on the stability of the solutions is a logical next step, the stability test provided in this thesis is not particularly persuasive and computationally inefficient. It is also unknown if the bifurcation diagrams are complete, the unsymmetrical solutions found in this thesis were mostly discovered based on a gut feeling that they would be there, so other solutions families might be missing from the diagrams. Videos of the evolution of the solutions in some of the bifurcation diagrams as well as code for plotting all the bifurcation diagrams and running the numerical simulations can be found in the GitHub repository [7].

References

[1] M. I. Budyko. The effect of solar radiation variations on the climate of the earth. *Tellus*, 21(5):611–619, 1969. `arXiv:https://doi.org/10.3402/tellusa.v21i5.10109`, `doi:10.3402/tellusa.v21i5.10109`.

[2] Gerald R. North. Analytical solution to a simple climate model with diffusive heat transport. *AMS Journal of the Atmospheric Sciences*, 32(7):1301–1307, 1975.

[3] Gerald R. North. Theory of energy-balance climate models. *AMS Journal of the Atmospheric Sciences*, 32(11):2033–2043, 1975.

[4] Wolfram Research, Inc. Mathematica, Version 13.0.0. Champaign, IL, 2021. URL: `https://www.wolfram.com/mathematica`.

[5] Jeremy Axelrod. Approximating the analytic fourier transform with the discrete fourier transform, 2015. URL: `https://arxiv.org/abs/1508.01282`, `doi:10.48550/ARXIV.1508.01282`.

[6] E. Isaacson and H.B. Keller. *Analysis of Numerical Methods*. Dover Books on Mathematics. Dover Publications, 1994. URL: `https://books.google.no/books?id=y77n2ySMJHUC`.

[7] Ask Elvevold. Master. URL: `https://github.com/GoodBoye98/Master`.

[8] Per Kristen Jakobsen. Boundary formulations for energy balance models in climate science. Notes from supervisor on energy balance models.

A Derivation of the model

To derive the model, lets start with some base quantities and define what they are [8]. First off, energy density $e(x,t)$. Which is defined at each point x and time t to be

$$\begin{aligned} e(x,t)dx \quad & \text{Energy at a small segment of length} \\ & dx \text{ on the line around } x \end{aligned} \tag{89}$$

Next up is the quantity that describes where energy flows $q(x,t)$, the energy flux density. In the 1D domain, this is just a scalar quantity and not a vector quantity as it's described as in the 2D case. It's simply just defined as

$$q(x,t) \tag{90}$$

where a positive q would mean energy is flowing to the right, and a negative value means it's flowing to the left. Lastly, another scalar quantity $h(x,t)$ that has the interpretation energy source density. This just means how much energy is absorbed or radiated at point x at time t.

$$\begin{aligned} h(x,t)dx \quad & \text{Energy is absorbed/radiated by} \\ & \text{segment } dx \text{ of the line around point } x \end{aligned} \tag{91}$$

With these quantities in mind, the domain of interest here is an infinite line. So these quantities will be considered on the unbounded real axis. Introduce the quantities $E(t)$ and $H(t)$, which describe the total amount of contained energy and total amount of absorbed or radiated energy respectively on a segment of the line. They are defined as

$$E(t) = \int_{L_0}^{L_1} e(x,t)dx \tag{92}$$

$$H(t) = \int_{L_0}^{L_1} h(x,t)dx \tag{93}$$

Now from the previous definitions, it's apparent that the change in energy must be

$$\frac{d}{dt}E(t) = H(t) - [q(x,t)]_{L_0}^{L_1} \tag{94}$$

Which can rewritten into

$$\begin{aligned} \partial_t \int_{L_0}^{L_1} dx e(x,t) &= \int_{L_0}^{L_1} dx h(x,t) - [q(x,t)]_{L_0}^{L_1} \\ \partial_t \int_{L_0}^{L_1} dx e(x,t) &= \int_{L_0}^{L_1} dx h(x,t) - \int_{L_0}^{L_1} dx \partial_x q(x,t) \\ \int_{L_0}^{L_1} dx \{\partial_t e(x,t) - h(x,t) + \partial_x q(x,t)\} &= 0 \end{aligned} \tag{95}$$

Because all of the calculations so far hold for any domain on the line, it must also hold that

$$\partial_t e(x,t) + \partial_x q(x,t) = h(x,t) \tag{96}$$

Which then must also hold on the entire real line. By then assuming that the system is in local thermodynamic equilibrium, the equation of state of the system takes form

$$e(x,t) = C(x,t)T(x,t) \tag{97}$$

where $C(x,t)$ is the heat capacity and $T(x,t)$ is the temperature at point x at time t. Now the energy flux density at a point x in this situation describes the transport of energy from said point to points infinitesimally close to x. From thermodynamics it's always true that energy flows from places of high temperature to places of low temperature, thus the energy flux density $q(x,t)$ is described as

$$q(x,t) = -K(x)\partial_x T(x), \quad K(x) > 0 \tag{98}$$

where $K(x)$ is the heat conductive parameter, this term usually varies from point to point so it is written here as a function of x. Next step is to combine the equations (96), (97) and (98) to get the equation

$$\partial_t(C(x,t)T(x,t)) = \partial_x(K(x,t)\partial_x T(x,t)) + h(x,t) \tag{99}$$

where $h(x,t)$ is defined as

$$h(x,t) = h_+(x)(1 - a(x,t)) - h_- \tag{100}$$

where h_+ is the solar radiation, $a(x,t)$ is the albedo of the surface and h_- is the energy returned to space as thermal radiation. However, it is misleading that the albedo is a function of x and t as it is dependent upon the temperature at each position. So from here and out it is written as a function of T instead. The next term in the equation is h_-, this is found by using the Stephen-Boltzmann law of black body radiation.

$$h_-(x,t) = \sigma T_k(x,t)^4 \tag{101}$$

Where σ is the Stephen-Boltzmann constant and $T_k(x,t)$, measured in Kelvin, is the thermodynamic temperature. However this temperature is not the same as the one down on the surface, but rather up in the atmosphere at the point where it's ability to scatter infrared radiation is too low. From that point and up radiation will be sent out of the system, the temperature in the atmosphere is not constant throughout itself, it decreases with height. This phenomenon is modelled by a linearized function around the temperature $T = 0°C$. Note that the temperature is measure in Celsius here and not Kelvin.

$$h_-(x,t) = A(x,t) + B(x,t)T(x,t) \tag{102}$$

A and B may vary from region to region and depending on what state the line is at said region, but the model does not suffer much from assuming they are constant. The incoming radiation-term $h_+(x,t)$ is modelled by

$$h(x)_+ = QS(x) \tag{103}$$

where Q is the solar constant and $S(x)$ is the radiation distribution function, which is a function determining how incoming solar radiation is distributed on the line. All of this combined gives the model used in this analysis.

$$C\partial_t T - \partial_x K \partial_x T = QS(1 - a(T)) - BT - A \tag{104}$$

Where the function T is measured in Celsius, note that the terms T_t and T_{xx} doesn't care about whether the model is in Celsius or Kelvin because they only care about temperature differences and not absolute temperature. And given that the BT term comes from a linearization using T measured in Celsius, it is most convenient to continue using Celsius as the unit of temperature.

B Boundary condition on continental edges

When computing the stationary solutions on the line containing a continent, a special type of boundary condition was used to determine the system. This boundary condition was on the derivatives of the temperature profile on each side of the continental edges, and the way it is found is by considering the first equation in (95).

$$\partial_t \int_{x_0}^{x_1} dx e(x,t) = \int_{x_0}^{x_1} dx h(x,t) - [q(x,t)]_{x_0}^{x_1} \tag{105}$$

This equation hold for any domain of the line, which means that it must also hold across the continental edges. The condition needed can be obtained from using this if it is considered around one of the continental edges. Say an edge is at the point $x = a$, then consider the equation on the domain $a - \epsilon$ to $a + \epsilon$. Note that this is considered only for stationary solutions, thus none of the terms are functions of t anymore.

$$\partial_t \int_{a-\epsilon}^{a+\epsilon} dx e(x) = \int_{a+\epsilon}^{a+\epsilon} dx h(x) - [q(x)]_{a+\epsilon}^{a+\epsilon} \tag{106}$$

The time derivative of a function of only x will be 0, putting the right hand side of the equation to 0. Next up is taking the limit as $\epsilon \to 0$

$$0 = \lim_{\epsilon \to 0} \int_{a+\epsilon}^{a+\epsilon} dx h(x,t) - q(a+\epsilon,t) + q(a-\epsilon,t) \tag{107}$$

The $h(x,t)$ function is piecewise smooth, which will make the integral go to 0 when $\epsilon \to 0$. Thus leaving only the q-term, rewriting the equation to right and left-sided limits gives

$$\lim_{x \to a^-} q(x,t) = \lim_{x \to a^+} q(x,t) \tag{108}$$

Now using equation (98) the special boundary condition for continental edges is obtained.

$$\lim_{x \to a^-} K(x) T_x(x) = \lim_{x \to a^+} K(x) T_x(x) \tag{109}$$

$K(x)$ only has two values in the application here, so this condition can take only two forms

$$\lim_{x \to a^-} K_w T_x(x) = \lim_{x \to a^+} K_l T_x(x) \tag{110}$$

for the case the continent on the right side of a, and

$$\lim_{x \to a^-} K_l T_x(x) = \lim_{x \to a^+} K_w T_x(x) \tag{111}$$

for when the continent is on the left side.

C List of boundary formulations

What follows is a list of all boundary formulations used in computing the different bifurcation diagrams. They are listed with the all the unknown quantities as well as the system of equations that is used to solve for the unknowns.

C.1 Ice

The simplest case, where the entire line is covered in ice. This is already covered in the main thesis, but it is here as well to make the list complete.

$$T(\xi) = \int_{-\infty}^{\infty} dx k_w(\eta_w S(1-a_0) - \alpha_w)$$

There are no unknown quantities here, a choice of Q and $S(x)$ gives the entire temperature profile. An example of a solution on this form is plotted in figure 30.

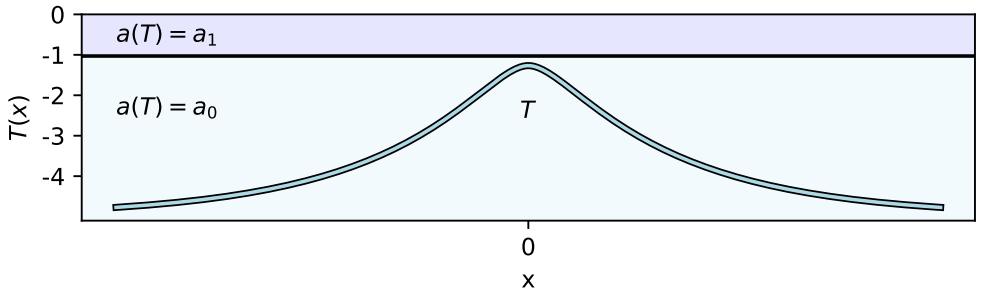

Figure 30: Example of solution "Ice"

C.2 IceWaterIce

This is the only other boundary formulation found in the case with no continent on the line. This solution is split into three regions.

$$T_1(\xi) = \Big[\partial_x T k_w - T\partial_x k_w\Big]_{-\infty}^{A_0} + \int_{-\infty}^{A_0} dx k_w(\eta_w S(1-a_0) - \alpha_w), \qquad -\infty < \xi < A_0$$

$$T_2(\xi) = \Big[\partial_x T k_w - T\partial_x k_w\Big]_{A_0}^{A_1} + \int_{A_0}^{A_1} dx k_w(\eta_w S(1-a_1) - \alpha_w), \qquad A_0 < \xi < A_1$$

$$T_3(\xi) = \Big[\partial_x T k_w - T\partial_x k_w\Big]_{A_1}^{\infty} + \int_{A_1}^{\infty} dx k_w(\eta_w S(1-a_0) - \alpha_w), \qquad A_1 < \xi < \infty$$

These equation has four unknown quantities.

$$T_x(A_0), T_x(A_1), A_0, A_1.$$

And the system of equations to solve for the quantities.

$$\lim_{\xi \to A_0^-} T_1(\xi) = -1,$$
$$\lim_{\xi \to A_0^+} T_2(\xi) = -1,$$
$$\lim_{\xi \to A_1^-} T_2(\xi) = -1,$$
$$\lim_{\xi \to A_1^+} T_3(\xi) = -1,$$

An example of a solution on this form is plotted in figure 31.

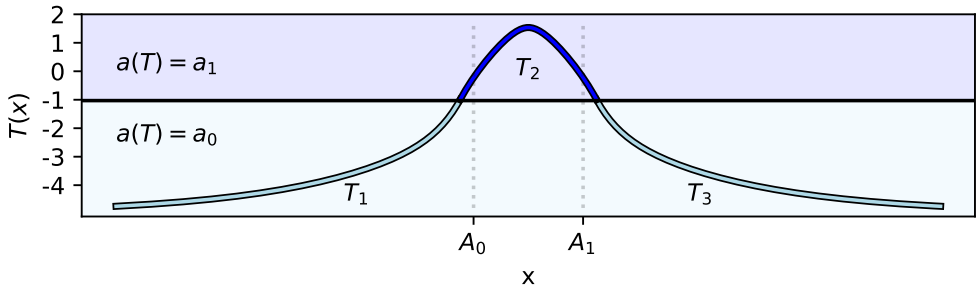

Figure 31: Example of solution "IceWaterIce"

C.3 IceSnowIce

The simplest boundary formulation for the case with a continent placed at (L_0, L_1). Consist of three regions, all with albedo a_0. However, the heat diffusion parameter, and thus the Greens function, differs between the regions covered in ice and the regions covered in snow.

$$T_1(\xi) = \Big[\partial_x T k_w - T\partial_x k_w\Big]_{-\infty}^{L_0} + \int_{-\infty}^{L_0} dx k_w(\eta_w S(1-a_0) - \alpha_w), \qquad -\infty < \xi < L_0$$

$$T_2(\xi) = \Big[\partial_x T k_l - T\partial_x k_l\Big]_{L_0}^{L_1} + \int_{L_0}^{L_1} dx k_l(\eta_l S(1-a_0) - \alpha_l), \qquad L_0 < \xi < L_1$$

$$T_3(\xi) = \Big[\partial_x T k_w - T\partial_x k_w\Big]_{L_1}^{\infty} + \int_{L_1}^{\infty} dx k_w(\eta_w S(1-a_0) - \alpha_w), \qquad L_1 < \xi < \infty$$

These include the unknown quantities.

$$T(L_0), T_x(L_0), T(L_1), T_x(L_1).$$

And the system of equations to solve for the quantities.

$$\begin{aligned}
\lim_{\xi \to L_0^-} T_1(\xi) &= \lim_{\xi \to L_0^+} T_2(\xi), \\
\lim_{\xi \to L_1^-} T_2(\xi) &= \lim_{\xi \to L_1^+} T_3(\xi), \\
\lim_{\xi \to L_0^-} K_w \partial_x T_1(\xi) &= \lim_{\xi \to L_0^+} K_l \partial_x T_2(\xi), \\
\lim_{\xi \to L_1^-} K_l \partial_x T_2(\xi) &= \lim_{\xi \to L_1^+} K_w \partial_x T_3(\xi).
\end{aligned}$$

An example of a solution on this form is plotted in figure 32.

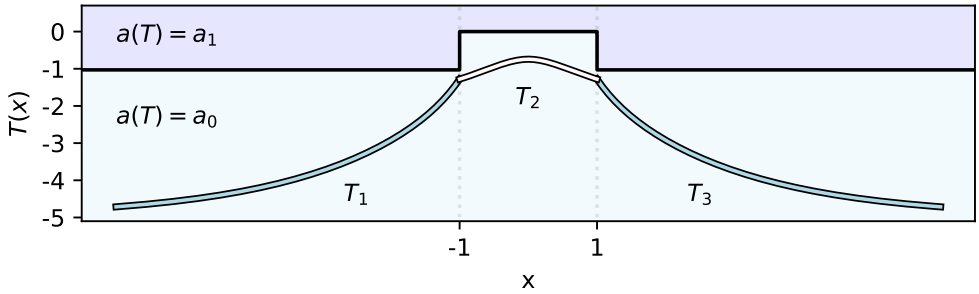

Figure 32: Example of solution "IceSnowIce"

C.4 IceWaterSnowWaterIce

This boundary formulation is fr the case with a continent placed at (L_0, L_1). The formulations are split into five regions, where some of the ice on each side of the continent has surpassed the critical temperature and melted into

water.

$$T_1(\xi) = \Big[\partial_x T k_w - T\partial_x k_w\Big]_{-\infty}^{A_0} + \int_{-\infty}^{A_0} dx k_w(\eta_w S(1-a_0) - \alpha_w), \qquad -\infty < \xi < A_0$$

$$T_2(\xi) = \Big[\partial_x T k_w - T\partial_x k_w\Big]_{A_0}^{L_0} + \int_{A_0}^{L_0} dx k_w(\eta_w S(1-a_1) - \alpha_w), \qquad A_0 < \xi < L_0$$

$$T_3(\xi) = \Big[\partial_x T k_l - T\partial_x k_l\Big]_{L_0}^{L_1} + \int_{L_0}^{L_1} dx k_l(\eta_l S(1-a_0) - \alpha_l), \qquad L_0 < \xi < L_1$$

$$T_4(\xi) = \Big[\partial_x T k_w - T\partial_x k_w\Big]_{L_1}^{A_1} + \int_{L_1}^{A_1} dx k_w(\eta_w S(1-a_1) - \alpha_w), \qquad L_1 < \xi < A_1$$

$$T_5(\xi) = \Big[\partial_x T k_w - T\partial_x k_w\Big]_{A_1}^{\infty} + \int_{A_1}^{\infty} dx k_w(\eta_w S(1-a_0) - \alpha_w), \qquad A_1 < \xi < \infty$$

These include the unknown quantities.

$$T_x(A_0), T(L_0), T_x(L_0), T(L_1), T_x(L_1), T_x(A_1), A_0, A_1.$$

And the system of equations to solve for the quantities.

$$\begin{aligned}
\lim_{\xi \to A_0^-} T_1(\xi) &= -1 \\
\lim_{\xi \to A_0^+} T_2(\xi) &= -1 \\
\lim_{\xi \to A_1^-} T_4(\xi) &= -1 \\
\lim_{\xi \to A_1^+} T_5(\xi) &= -1 \\
\lim_{\xi \to L_0^-} T_2(\xi) &= \lim_{\xi \to L_0^+} T_3(\xi), \\
\lim_{\xi \to L_1^-} T_3(\xi) &= \lim_{\xi \to L_1^+} T_4(\xi), \\
\lim_{\xi \to L_0^-} K_w \partial_x T_2(\xi) &= \lim_{\xi \to L_0^+} K_l \partial_x T_3(\xi), \\
\lim_{\xi \to L_1^-} K_l \partial_x T_3(\xi) &= \lim_{\xi \to L_1^+} K_w \partial_x T_4(\xi).
\end{aligned}$$

This system is very difficult to solve analytically, so a numeric root finding algorithm was used instead. An example of a solution on this form is plotted in figure 33

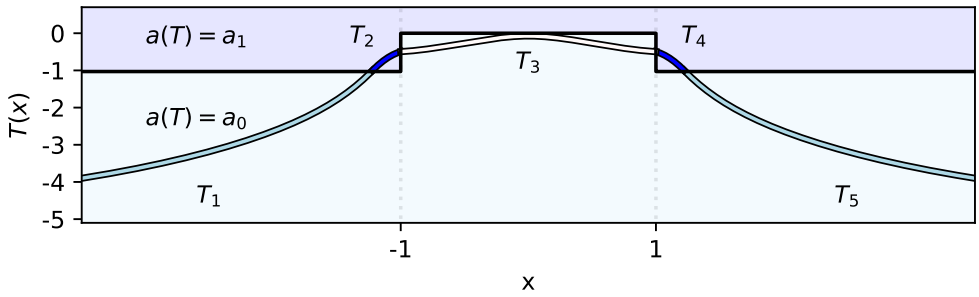

Figure 33: Example of solution "IceWaterSnowWaterIce"

C.5 IceWaterSnowLandSnowWaterIce

This boundary formulation is a special case of the 2N-boundary formulation that comes last. It is also the longest one that is formulated explicitly. It consists of seven regions, where the critical temperature is crossed both on the

continent and on both sides as well.

$$
\begin{aligned}
T_1(\xi) &= \Big[\partial_x T k_w - T\partial_x k_w\Big]_{-\infty}^{A_0} + \int_{-\infty}^{A_0} dx k_w(\eta_w S(1-a_0) - \alpha_w), && -\infty < \xi < A_0 \\
T_2(\xi) &= \Big[\partial_x T k_w - T\partial_x k_w\Big]_{A_0}^{L_0} + \int_{A_0}^{L_0} dx k_w(\eta_w S(1-a_1) - \alpha_w), && A_0 < \xi < L_0 \\
T_3(\xi) &= \Big[\partial_x T k_l - T\partial_x k_l\Big]_{L_0}^{B_0} + \int_{L_0}^{B_0} dx k_l(\eta_l S(1-a_0) - \alpha_l), && L_0 < \xi < B_0 \\
T_4(\xi) &= \Big[\partial_x T k_l - T\partial_x k_l\Big]_{B_0}^{B_1} + \int_{B_0}^{B_1} dx k_l(\eta_l S(1-a_1) - \alpha_l), && B_0 < \xi < B_1 \\
T_5(\xi) &= \Big[\partial_x T k_l - T\partial_x k_l\Big]_{B_1}^{L_1} + \int_{B_1}^{L_1} dx k_l(\eta_l S(1-a_0) - \alpha_l), && B_1 < \xi < L_1 \\
T_6(\xi) &= \Big[\partial_x T k_w - T\partial_x k_w\Big]_{L_1}^{A_1} + \int_{L_1}^{A_1} dx k_w(\eta_w S(1-a_1) - \alpha_w), && L_1 < \xi < A_1 \\
T_7(\xi) &= \Big[\partial_x T k_w - T\partial_x k_w\Big]_{A_1}^{\infty} + \int_{A_1}^{\infty} dx k_w(\eta_w S(1-a_0) - \alpha_w), && A_1 < \xi < \infty
\end{aligned}
$$

These include the unknown quantities.

$$T_x(A_0), T(L_0), T_x(L_0), T_x(B_0), T_x(B_1), T(L_1), T_x(L_1), T_x(A_1), A_0, A_1, B_0, B_1.$$

And the system of equations to solve for the quantities.

$$
\begin{aligned}
\lim_{\xi \to A_0^-} T_1(\xi) &= -1, \\
\lim_{\xi \to A_0^+} T_2(\xi) &= -1, \\
\lim_{\xi \to A_1^-} T_6(\xi) &= -1, \\
\lim_{\xi \to A_1^+} T_7(\xi) &= -1, \\
\lim_{\xi \to B_0^-} T_3(\xi) &= 0, \\
\lim_{\xi \to B_0^+} T_4(\xi) &= 0, \\
\lim_{\xi \to B_1^-} T_4(\xi) &= 0, \\
\lim_{\xi \to B_1^+} T_5(\xi) &= 0, \\
\lim_{\xi \to L_0^-} T_2(\xi) &= \lim_{\xi \to L_0^+} T_3(\xi), \\
\lim_{\xi \to L_1^-} T_5(\xi) &= \lim_{\xi \to L_1^+} T_6(\xi), \\
\lim_{\xi \to L_0^-} K_w \partial_x T_2(\xi) &= \lim_{\xi \to L_0^+} K_l \partial_x T_3(\xi), \\
\lim_{\xi \to L_1^-} K_l \partial_x T_5(\xi) &= \lim_{\xi \to L_1^+} K_w \partial_x T_6(\xi).
\end{aligned}
$$

There are also solved by using a numerical root finding algorithm. An example of a solution on this form is plotted in figure 34.

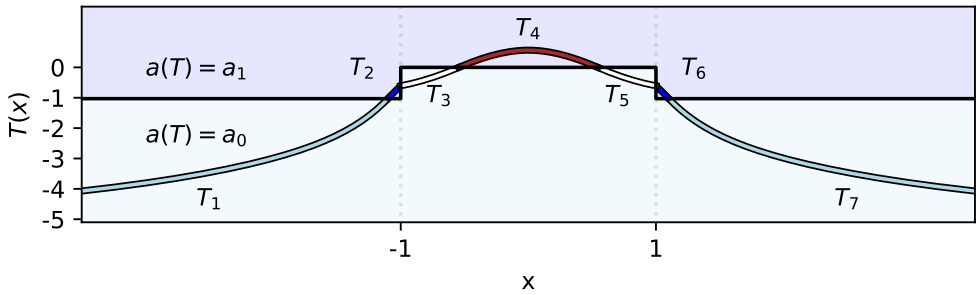

Figure 34: Example of solution "IceWaterSnowLandSnowWaterIce"

C.6 IceWaterLandWaterIce

This boundary formulation is used when all the snow on the continent has melted. It is the only one has solutions for an arbitrarily high value of Q, apart from the IceWaterIce formulation in the case without a continent. The formulation is almost identical to the IceWaterSnowWaterIce boundary solution, the only difference being in T_3, where a_0 has been replaced with a_1.

$$
\begin{aligned}
T_1(\xi) &= \Big[\partial_x T k_w - T\partial_x k_w\Big]_{-\infty}^{A_0} + \int_{-\infty}^{A_0} dx k_w(\eta_w S(1-a_0) - \alpha_w), \qquad -\infty < \xi < A_0 \\
T_2(\xi) &= \Big[\partial_x T k_w - T\partial_x k_w\Big]_{A_0}^{L_0} + \int_{A_0}^{L_0} dx k_w(\eta_w S(1-a_1) - \alpha_w), \qquad A_0 < \xi < L_0 \\
T_3(\xi) &= \Big[\partial_x T k_l - T\partial_x k_l\Big]_{L_0}^{L_1} + \int_{L_0}^{L_1} dx k_l(\eta_l S(1-a_1) - \alpha_l), \qquad L_0 < \xi < L_1 \\
T_4(\xi) &= \Big[\partial_x T k_w - T\partial_x k_w\Big]_{L_1}^{A_1} + \int_{L_1}^{A_1} dx k_w(\eta_w S(1-a_1) - \alpha_w), \qquad L_1 < \xi < A_1 \\
T_5(\xi) &= \Big[\partial_x T k_w - T\partial_x k_w\Big]_{A_1}^{\infty} + \int_{A_1}^{\infty} dx k_w(\eta_w S(1-a_0) - \alpha_w), \qquad A_1 < \xi < \infty
\end{aligned}
$$

These include the unknown quantities.

$$
T_x(A_0), T(L_0), T_x(L_0), T(L_1), T_x(L_1), T_x(A_1), A_0, A_1.
$$

And the system of equations to solve for the quantities.

$$
\begin{aligned}
\lim_{\xi \to A_0^-} T_1(\xi) &= -1 \\
\lim_{\xi \to A_0^+} T_2(\xi) &= -1 \\
\lim_{\xi \to A_1^-} T_4(\xi) &= -1 \\
\lim_{\xi \to A_1^+} T_5(\xi) &= -1 \\
\lim_{\xi \to L_0^-} T_2(\xi) &= \lim_{\xi \to L_0^+} T_3(\xi), \\
\lim_{\xi \to L_1^-} T_3(\xi) &= \lim_{\xi \to L_1^+} T_4(\xi), \\
\lim_{\xi \to L_0^-} K_w \partial_x T_2(\xi) &= \lim_{\xi \to L_0^+} K_l \partial_x T_3(\xi), \\
\lim_{\xi \to L_1^-} K_l \partial_x T_3(\xi) &= \lim_{\xi \to L_1^+} K_w \partial_x T_4(\xi).
\end{aligned}
$$

This system is also solved for by using a numerical root finding algorithm. An example of a solution on this form is plotted in figure 35.

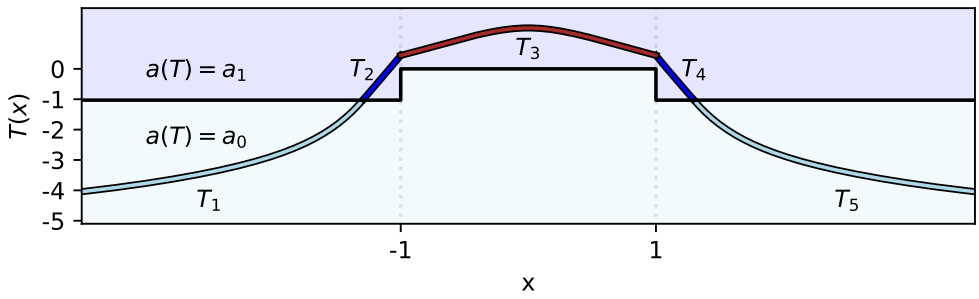

Figure 35: Example of solution "IceWaterLandWaterIce"

C.7 IceWaterSnowIce

This is the first boundary formulation that assumes a unsymmetrical solution. It assumes that ice has melted on only one side of the continent. In this thesis the continent is placed at $(-1+\epsilon, 1+\epsilon)$, where $\epsilon \leq 0$. Thus having the left

side of the continent being the one that is melted makes sense.

$$
\begin{aligned}
T_1(\xi) &= \Big[\partial_x T k_w - T\partial_x k_w\Big]_{-\infty}^{A_0} + \int_{-\infty}^{A_0} dx k_w(\eta_w S(1-a_0) - \alpha_w), && -\infty < \xi < A_0 \\
T_2(\xi) &= \Big[\partial_x T k_w - T\partial_x k_w\Big]_{A_0}^{L_0} + \int_{A_0}^{L_0} dx k_w(\eta_w S(1-a_1) - \alpha_w), && A_0 < \xi < L_0 \\
T_3(\xi) &= \Big[\partial_x T k_l - T\partial_x k_l\Big]_{L_0}^{L_1} + \int_{L_0}^{L_1} dx k_l(\eta_l S(1-a_0) - \alpha_l), && L_0 < \xi < L_1 \\
T_4(\xi) &= \Big[\partial_x T k_w - T\partial_x k_w\Big]_{L_1}^{\infty} + \int_{L_1}^{\infty} dx k_w(\eta_w S(1-a_0) - \alpha_w), && L_1 < \xi < \infty
\end{aligned}
$$

These include the unknown quantities.

$$T_x(A_0), T(L_0), T_x(L_0), T(L_1), T_x(L_1), A_0.$$

And the system of equations to solve for the quantities.

$$
\begin{aligned}
\lim_{\xi \to A_0^-} T_1(\xi) &= -1 \\
\lim_{\xi \to A_0^+} T_2(\xi) &= -1 \\
\lim_{\xi \to L_0^-} T_2(\xi) &= \lim_{\xi \to L_0^+} T_3(\xi), \\
\lim_{\xi \to L_1^-} T_3(\xi) &= \lim_{\xi \to L_1^+} T_4(\xi), \\
\lim_{\xi \to L_0^-} K_w \partial_x T_2(\xi) &= \lim_{\xi \to L_0^+} K_l \partial_x T_3(\xi), \\
\lim_{\xi \to L_1^-} K_l \partial_x T_3(\xi) &= \lim_{\xi \to L_1^+} K_w \partial_x T_4(\xi).
\end{aligned}
$$

Like before, this system is solved by using a numerical root finding algorithm. And an example of a solution on this form is plotted in figure 36.

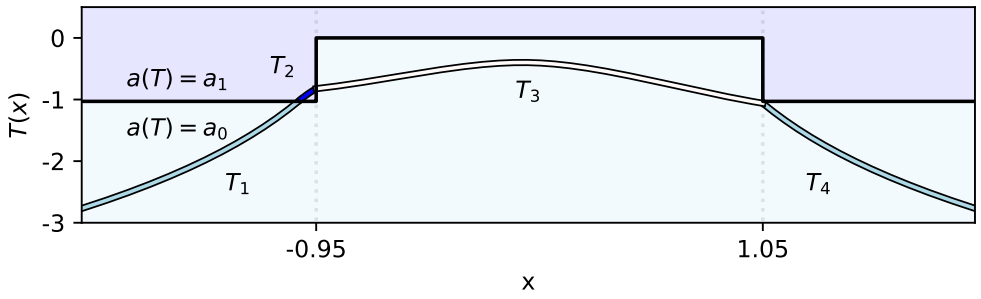

Figure 36: Example of solution "IceWaterSnowIce"

C.8 IceWaterSnowLandSnowIce

A more complicated boundary formulation that assumes unsymmetrical solutions. This is mostly the same as the previous one, except that a region of the continent has melted as well.

$$
\begin{aligned}
T_1(\xi) &= \Big[\partial_x T k_w - T\partial_x k_w\Big]_{-\infty}^{A_0} + \int_{-\infty}^{A_0} dx k_w(\eta_w S(1-a_0) - \alpha_w), && -\infty < \xi < A_0 \\
T_2(\xi) &= \Big[\partial_x T k_w - T\partial_x k_w\Big]_{A_0}^{L_0} + \int_{A_0}^{L_0} dx k_w(\eta_w S(1-a_1) - \alpha_w), && A_0 < \xi < L_0 \\
T_3(\xi) &= \Big[\partial_x T k_l - T\partial_x k_l\Big]_{L_0}^{B_0} + \int_{L_0}^{B_0} dx k_l(\eta_l S(1-a_0) - \alpha_l), && L_0 < \xi < B_0 \\
T_4(\xi) &= \Big[\partial_x T k_l - T\partial_x k_l\Big]_{B_0}^{B_1} + \int_{B_0}^{B_1} dx k_l(\eta_l S(1-a_1) - \alpha_l), && B_0 < \xi < B_1 \\
T_5(\xi) &= \Big[\partial_x T k_l - T\partial_x k_l\Big]_{B_1}^{L_1} + \int_{B_1}^{L_1} dx k_l(\eta_l S(1-a_0) - \alpha_l), && B_1 < \xi < L_1 \\
T_6(\xi) &= \Big[\partial_x T k_w - T\partial_x k_w\Big]_{L_1}^{\infty} + \int_{L_1}^{\infty} dx k_w(\eta_w S(1-a_0) - \alpha_w), && L_1 < \xi < \infty
\end{aligned}
$$

These include the unknown quantities.

$$T_x(A_0), T(L_0), T_x(L_0), T_x(B_0), T_x(B_1), T(L_1), T_x(L_1), A_0, B_0, B_1.$$

And the system of equations to solve for the quantities.

$$\begin{aligned}
\lim_{\xi \to A_0^-} T_1(\xi) &= -1 \\
\lim_{\xi \to A_0^+} T_2(\xi) &= -1 \\
\lim_{\xi \to B_0^-} T_3(\xi) &= 0 \\
\lim_{\xi \to B_0^+} T_4(\xi) &= 0 \\
\lim_{\xi \to B_1^-} T_4(\xi) &= 0 \\
\lim_{\xi \to B_1^+} T_5(\xi) &= 0 \\
\lim_{\xi \to L_0^-} T_2(\xi) &= \lim_{\xi \to L_0^+} T_3(\xi), \\
\lim_{\xi \to L_1^-} T_5(\xi) &= \lim_{\xi \to L_1^+} T_6(\xi), \\
\lim_{\xi \to L_0^-} K_w \partial_x T_2(\xi) &= \lim_{\xi \to L_0^+} K_l \partial_x T_3(\xi), \\
\lim_{\xi \to L_1^-} K_l \partial_x T_5(\xi) &= \lim_{\xi \to L_1^+} K_w \partial_x T_6(\xi).
\end{aligned}$$

Like before, this system is solved by using a numerical root finding algorithm. And an example of a solution on this form is plotted in figure 38.

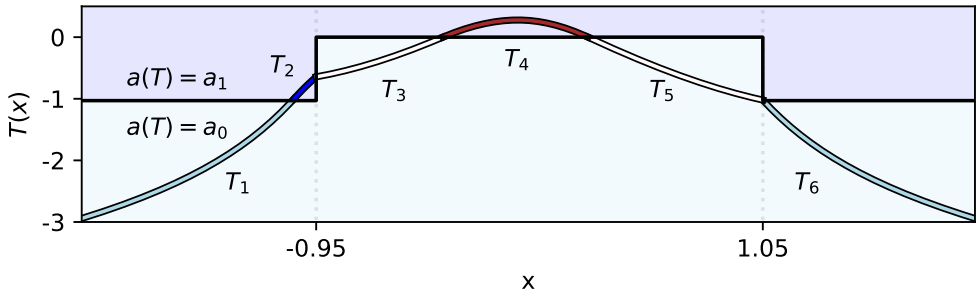

Figure 37: Example of solution "IceWaterSnowLandSnowIce"

C.9 IceWaterLandSnowWaterIce

This is the first boundary formulation where the assumed asymmetry lies on the continent, here the left part of the continent has melted, while the right part of the continent is covered in snow.

$$\begin{aligned}
T_1(\xi) &= \Big[\partial_x T k_w - T \partial_x k_w\Big]_{-\infty}^{A_0} + \int_{-\infty}^{A_0} dx k_w(\eta_w S(1-a_0) - \alpha_w), && -\infty < \xi < A_0 \\
T_2(\xi) &= \Big[\partial_x T k_w - T \partial_x k_w\Big]_{A_0}^{L_0} + \int_{A_0}^{L_0} dx k_w(\eta_w S(1-a_1) - \alpha_w), && A_0 < \xi < L_0 \\
T_3(\xi) &= \Big[\partial_x T k_l - T \partial_x k_l\Big]_{L_0}^{B_0} + \int_{L_0}^{B_0} dx k_l(\eta_l S(1-a_1) - \alpha_l), && L_0 < \xi < B_0 \\
T_4(\xi) &= \Big[\partial_x T k_l - T \partial_x k_l\Big]_{B_0}^{L_1} + \int_{B_0}^{L_1} dx k_l(\eta_l S(1-a_0) - \alpha_l), && B_0 < \xi < L_1 \\
T_5(\xi) &= \Big[\partial_x T k_w - T \partial_x k_w\Big]_{L_1}^{A_1} + \int_{L_1}^{A_1} dx k_w(\eta_w S(1-a_1) - \alpha_w), && L_1 < \xi < A_1 \\
T_6(\xi) &= \Big[\partial_x T k_w - T \partial_x k_w\Big]_{A_1}^{\infty} + \int_{A_1}^{\infty} dx k_w(\eta_w S(1-a_0) - \alpha_w), && A_1 < \xi < \infty
\end{aligned}$$

These include the unknown quantities.

$$T_x(A_0), T(L_0), T_x(L_0), T_x(B_0), T(L_1), T_x(L_1), T_x(A_1), A_0, A_1, B_0.$$

And the system of equations to solve for the quantities.

$$
\begin{aligned}
\lim_{\xi \to A_0^-} T_1(\xi) &= -1 \\
\lim_{\xi \to A_0^+} T_2(\xi) &= -1 \\
\lim_{\xi \to B_0^-} T_3(\xi) &= 0 \\
\lim_{\xi \to B_0^+} T_4(\xi) &= 0 \\
\lim_{\xi \to A_1^-} T_5(\xi) &= -1 \\
\lim_{\xi \to A_1^+} T_6(\xi) &= -1 \\
\lim_{\xi \to L_0^-} T_2(\xi) &= \lim_{\xi \to L_0^+} T_3(\xi), \\
\lim_{\xi \to L_1^-} T_4(\xi) &= \lim_{\xi \to L_1^+} T_5(\xi), \\
\lim_{\xi \to L_0^-} K_w \partial_x T_2(\xi) &= \lim_{\xi \to L_0^+} K_l \partial_x T_3(\xi), \\
\lim_{\xi \to L_1^-} K_l \partial_x T_4(\xi) &= \lim_{\xi \to L_1^+} K_w \partial_x T_5(\xi).
\end{aligned}
$$

Like before, this system is solved by using a numerical root finding algorithm. And an example of a solution on this form is plotted in figure 37.

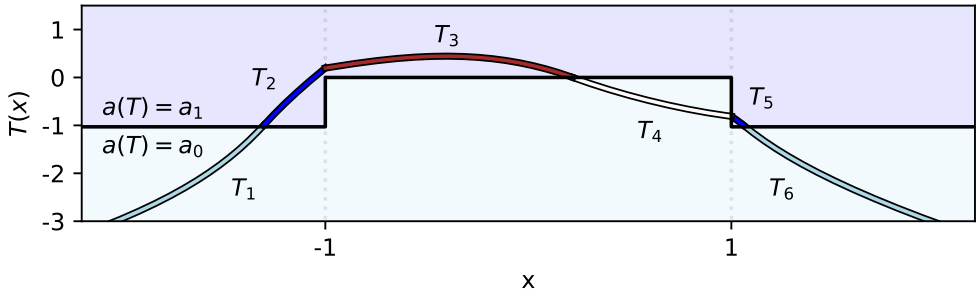

Figure 38: Example of solution "IceWaterLandSnowWaterIce"

C.10 IceWaterSnowLandWaterIce

This boundary formulation is just a mirror of the previous one. The only difference is that the a_0 and a_1 are swapped between T_3 and T_4. Otherwise everything is the same.

$$
\begin{aligned}
T_1(\xi) &= \Big[\partial_x T k_w - T \partial_x k_w\Big]_{-\infty}^{A_0} + \int_{-\infty}^{A_0} dx k_w(\eta_w S(1-a_0) - \alpha_w), && -\infty < \xi < A_0 \\
T_2(\xi) &= \Big[\partial_x T k_w - T \partial_x k_w\Big]_{A_0}^{L_0} + \int_{A_0}^{L_0} dx k_w(\eta_w S(1-a_1) - \alpha_w), && A_0 < \xi < L_0 \\
T_3(\xi) &= \Big[\partial_x T k_l - T \partial_x k_l\Big]_{L_0}^{B_0} + \int_{L_0}^{B_0} dx k_l(\eta_l S(1-a_0) - \alpha_l), && L_0 < \xi < B_0 \\
T_4(\xi) &= \Big[\partial_x T k_l - T \partial_x k_l\Big]_{B_0}^{L_1} + \int_{B_0}^{L_1} dx k_l(\eta_l S(1-a_1) - \alpha_l), && B_0 < \xi < L_1 \\
T_5(\xi) &= \Big[\partial_x T k_w - T \partial_x k_w\Big]_{L_1}^{A_1} + \int_{L_1}^{A_1} dx k_w(\eta_w S(1-a_1) - \alpha_w), && L_1 < \xi < A_1 \\
T_6(\xi) &= \Big[\partial_x T k_w - T \partial_x k_w\Big]_{A_1}^{\infty} + \int_{A_1}^{\infty} dx k_w(\eta_w S(1-a_0) - \alpha_w), && A_1 < \xi < \infty
\end{aligned}
$$

These include the unknown quantities.

$$
T_x(A_0), T(L_0), T_x(L_0), T_x(B_0), T(L_1), T_x(L_1), T_x(A_1), A_0, A_1, B_0.
$$

And the system of equations to solve for the quantities.

$$
\begin{aligned}
\lim_{\xi \to A_0^-} T_1(\xi) &= -1 \\
\lim_{\xi \to A_0^+} T_2(\xi) &= -1 \\
\lim_{\xi \to B_0^-} T_3(\xi) &= 0 \\
\lim_{\xi \to B_0^+} T_4(\xi) &= 0 \\
\lim_{\xi \to A_1^-} T_5(\xi) &= -1 \\
\lim_{\xi \to A_1^+} T_6(\xi) &= -1 \\
\lim_{\xi \to L_0^-} T_2(\xi) &= \lim_{\xi \to L_0^+} T_3(\xi), \\
\lim_{\xi \to L_1^-} T_4(\xi) &= \lim_{\xi \to L_1^+} T_5(\xi), \\
\lim_{\xi \to L_0^-} K_w \partial_x T_2(\xi) &= \lim_{\xi \to L_0^+} K_l \partial_x T_3(\xi), \\
\lim_{\xi \to L_1^-} K_l \partial_x T_4(\xi) &= \lim_{\xi \to L_1^+} K_w \partial_x T_5(\xi).
\end{aligned}
$$

Like before, this system is solved by using a numerical root finding algorithm. And an example of a solution on this form is plotted in figure 39.

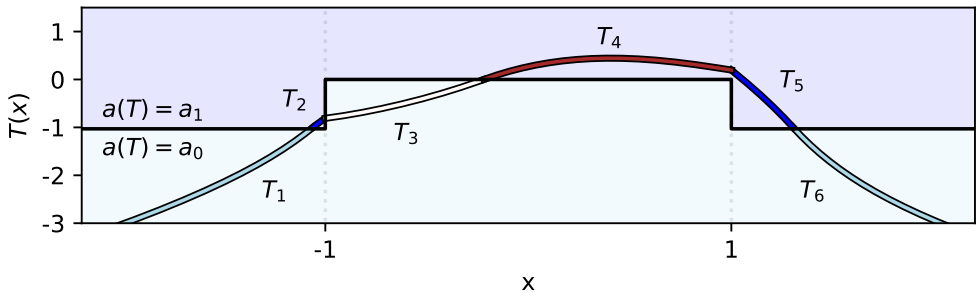

Figure 39: Example of solution "IceWaterSnowLandWaterIce"

C.11 IceWaterLandSnowIce

This boundary formulation is also similar to the previous one, except this one is missing water of the right side of the continent.

$$
\begin{aligned}
T_1(\xi) &= \Big[\partial_x T k_w - T \partial_x k_w\Big]_{-\infty}^{A_0} + \int_{-\infty}^{A_0} dx k_w(\eta_w S(1-a_0) - \alpha_w), \qquad -\infty < \xi < A_0 \\
T_2(\xi) &= \Big[\partial_x T k_w - T \partial_x k_w\Big]_{A_0}^{L_0} + \int_{A_0}^{L_0} dx k_w(\eta_w S(1-a_1) - \alpha_w), \qquad A_0 < \xi < L_0 \\
T_3(\xi) &= \Big[\partial_x T k_l - T \partial_x k_l\Big]_{L_0}^{B_0} + \int_{L_0}^{B_0} dx k_l(\eta_l S(1-a_0) - \alpha_l), \qquad L_0 < \xi < B_0 \\
T_4(\xi) &= \Big[\partial_x T k_l - T \partial_x k_l\Big]_{B_0}^{L_1} + \int_{B_0}^{L_1} dx k_l(\eta_l S(1-a_1) - \alpha_l), \qquad B_0 < \xi < L_1 \\
T_5(\xi) &= \Big[\partial_x T k_w - T \partial_x k_w\Big]_{L_0}^{\infty} + \int_{L_0}^{\infty} dx k_w(\eta_w S(1-a_0) - \alpha_w), \qquad L_1 < \xi < \infty
\end{aligned}
$$

These include the unknown quantities.

$$
T_x(A_0), T(L_0), T_x(L_0), T_x(B_0), T(L_1), T_x(L_1), A_0, B_0.
$$

And the system of equations to solve for the quantities.

$$
\begin{aligned}
\lim_{\xi \to A_0^-} T_1(\xi) &= -1 \\
\lim_{\xi \to A_0^+} T_2(\xi) &= -1 \\
\lim_{\xi \to B_0^-} T_3(\xi) &= 0 \\
\lim_{\xi \to B_0^+} T_4(\xi) &= 0 \\
\lim_{\xi \to L_0^-} T_2(\xi) &= \lim_{\xi \to L_0^+} T_3(\xi), \\
\lim_{\xi \to L_1^-} T_4(\xi) &= \lim_{\xi \to L_1^+} T_5(\xi), \\
\lim_{\xi \to L_0^-} K_w \partial_x T_2(\xi) &= \lim_{\xi \to L_0^+} K_l \partial_x T_3(\xi), \\
\lim_{\xi \to L_1^-} K_l \partial_x T_4(\xi) &= \lim_{\xi \to L_1^+} K_w \partial_x T_5(\xi).
\end{aligned}
$$

Like before, this system is solved by using a numerical root finding algorithm. And an example of a solution on this form is plotted in figure 40.

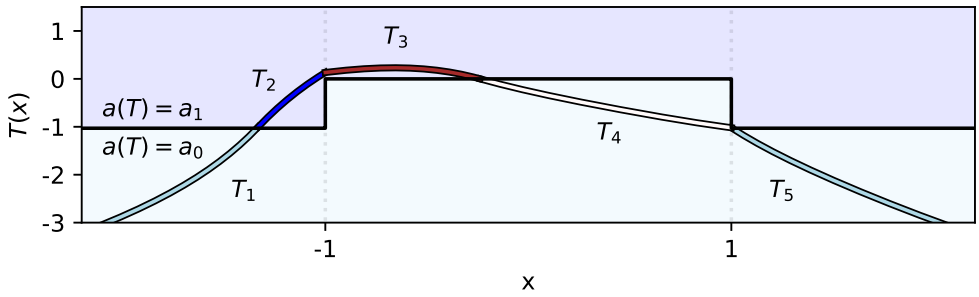

Figure 40: Example of solution "IceWaterLandSnowIce"

C.12 IceSnowLandWaterIce

This is a mirror of the previous boundary formulation. The water is now on the right side of the continent, and the left part of the continent is melted instead of the right.

$$
\begin{aligned}
T_1(\xi) &= \Big[\partial_x T k_w - T \partial_x k_w\Big]_{-\infty}^{L_0} + \int_{-\infty}^{L_0} dx k_w(\eta_w S(1-a_0) - \alpha_w), && -\infty < \xi < L_0 \\
T_2(\xi) &= \Big[\partial_x T k_l - T \partial_x k_l\Big]_{L_0}^{B_0} + \int_{L_0}^{B_0} dx k_l(\eta_l S(1-a_1) - \alpha_l), && L_0 < \xi < B_0 \\
T_3(\xi) &= \Big[\partial_x T k_l - T \partial_x k_l\Big]_{B_0}^{L_1} + \int_{B_0}^{L_1} dx k_l(\eta_l S(1-a_0) - \alpha_l), && B_0 < \xi < L_1 \\
T_4(\xi) &= \Big[\partial_x T k_w - T \partial_x k_w\Big]_{L_1}^{A_1} + \int_{L_1}^{A_1} dx k_w(\eta_w S(1-a_1) - \alpha_w), && L_1 < \xi < A_1 \\
T_5(\xi) &= \Big[\partial_x T k_w - T \partial_x k_w\Big]_{A_1}^{\infty} + \int_{A_1}^{\infty} dx k_w(\eta_w S(1-a_0) - \alpha_w), && A_1 < \xi < \infty
\end{aligned}
$$

These include the unknown quantities.

$$T_x(A_0), T(L_0), T_x(L_0), T_x(B_0), T(L_1), T_x(L_1), A_1, B_0.$$

And the system of equations to solve for the quantities.

$$\begin{aligned}
\lim_{\xi\to B_0^-} T_2(\xi) &= 0\\
\lim_{\xi\to B_0^+} T_3(\xi) &= 0\\
\lim_{\xi\to A_1^-} T_4(\xi) &= -1\\
\lim_{\xi\to A_1^+} T_5(\xi) &= -1\\
\lim_{\xi\to L_0^-} T_1(\xi) &= \lim_{\xi\to L_0^+} T_2(\xi),\\
\lim_{\xi\to L_1^-} T_3(\xi) &= \lim_{\xi\to L_1^+} T_4(\xi),\\
\lim_{\xi\to L_0^-} K_w\partial_x T_1(\xi) &= \lim_{\xi\to L_0^+} K_l\partial_x T_2(\xi),\\
\lim_{\xi\to L_1^-} K_l\partial_x T_3(\xi) &= \lim_{\xi\to L_1^+} K_w\partial_x T_4(\xi).
\end{aligned}$$

Like before, this system is solved by using a numerical root finding algorithm. And an example of a solution on this form is plotted in figure 41.

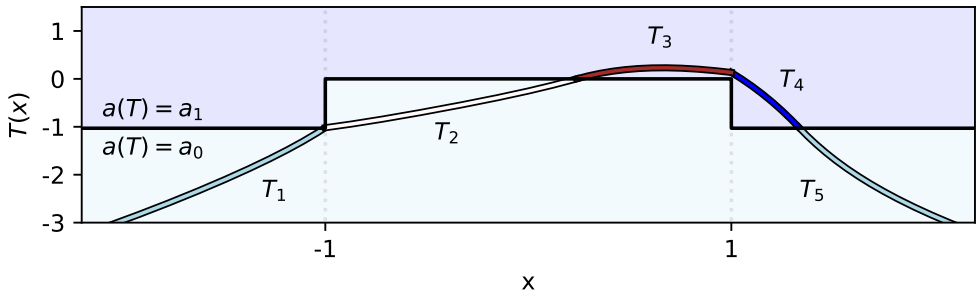

Figure 41: Example of solution "IceSnowLandWaterIce"

C.13 General 2N-boundary formulation

The last boundary formulation that is used in the computation of the bifurcation diagrams is the 2N-boundary formulation. This is a general, symmetrical boundary formulation for an arbitrary number of snow-land transitions on the continent. Doing this generally is especially useful in computing the bifurcation diagram in the gaussian case depicted in figure 18. To do this, the first step is to separate the boundary formulations for the regions with water from the region with a continent. On the left side of the continent the equations that model the temperature are

$$\begin{aligned}
T_{-2}(\xi) &= \Big[\partial_x T k_w - T\partial_x k_w\Big]_{-\infty}^{A_0} + \int_{-\infty}^{A_0} dx k_w(\eta_w S(1-a_0) - \alpha_w), \qquad -\infty < \xi < A_0\\
T_{-1}(\xi) &= \Big[\partial_x T k_w - T\partial_x k_w\Big]_{A_0}^{L_0} + \int_{A_0}^{L_0} dx k_w(\eta_w S(1-a_1) - \alpha_w), \qquad A_0 < \xi < L_0
\end{aligned}$$

And on the right side of the continent

$$\begin{aligned}
T_1(\xi) &= \Big[\partial_x T k_w - T\partial_x k_w\Big]_{L_1}^{A_1} + \int_{L_1}^{A_1} dx k_w(\eta_w S(1-a_1) - \alpha_w), \qquad L_1 < \xi < A_1\\
T_2(\xi) &= \Big[\partial_x T k_w - T\partial_x k_w\Big]_{A_1}^{\infty} + \int_{A_1}^{\infty} dx k_w(\eta_w S(1-a_0) - \alpha_w), \qquad A_1 < \xi < \infty
\end{aligned}$$

These are constant no matter how many snow-edges are on the continent. These equations include the eight unknown quantities

$$T_x(A_0), T(L_0), T_x(L_0), T(L_1), T_x(L_1), T_x(A_1), A_0, A_1.$$

Furthermore, by introducing $2N$ snow-edges on the continent, $2N+1$ equations are needed to model the entire domain, $G_i(\xi)$, $i = -N, \ldots, -1, 0, 1, \ldots, N$. These are constructed as follows

$$
\begin{aligned}
G_0(\xi) &= \Big[\partial_x T k_l - T\partial_x k_l\Big]_{B_{-1}}^{B_1} + \int_{B_{-1}}^{B_1} dx k_l(\eta_l S(1 - a_{c(l)}) - \alpha_l), \qquad B_{-1} < \xi < B_1 \\
G_N(\xi) &= \Big[\partial_x T k_l - T\partial_x k_l\Big]_{B_N}^{L_1} + \int_{B_N}^{L_1} dx k_l(\eta_l S(1 - a_{c(N+l)}) - \alpha_l), \qquad B_N < \xi < L_1 \\
G_{-N}(\xi) &= \Big[\partial_x T k_l - T\partial_x k_l\Big]_{L_0}^{B_{-N}} + \int_{L_0}^{B_{-N}} dx k_l(\eta_l S(1 - a_{c(N+l)}) - \alpha_l), \qquad L_0 < \xi < B_{-N} \\
c(x) &= \begin{cases} 0, & \text{x is even} \\ 1, & \text{x is odd} \end{cases}
\end{aligned}
$$

For the static cases, the ones that exist for all $N > 0$. And the rest are

$$
\begin{aligned}
G_i(\xi) &= \Big[\partial_x T k_l - T\partial_x k_l\Big]_{B_i}^{B_{i+1}} + \int_{B_i}^{B_{i+1}} dx k_l(\eta_l S(1 - a_{c(i+l)}) - \alpha_l), \qquad B_i < \xi < B_{i+1} \\
G_{-i}(\xi) &= \Big[\partial_x T k_l - T\partial_x k_l\Big]_{B_{-i-1}}^{B_{-i}} + \int_{B_{-i-1}}^{B_{-i}} dx k_l(\eta_l S(1 - a_{c(i+l)}) - \alpha_l), \qquad B_{-i-1} < \xi < B_{-i} \\
i &= 1, 2, \ldots, N-1,
\end{aligned}
$$

Thus if $l = 0$, the centre of the continent is covered in snow, and if $l = 1$ the centre is land. These new equations introduce $4N$ new unknown quantities

$$B_i, B_{-i}, T_x(B_i), T_x(B_{-i}), i = 1, 2, \ldots, N.$$

Which means that the total number of unknown quantities in these equations is $4N+8$. The static system of equation, the ones that exist for any $N > 0$ are as follows

$$
\begin{aligned}
\lim_{\xi \to A_0^-} T_{-2}(\xi) &= -1 \\
\lim_{\xi \to A_0^+} T_{-1}(\xi) &= -1 \\
\lim_{\xi \to A_1^-} T_1(\xi) &= -1 \\
\lim_{\xi \to A_1^+} T_2(\xi) &= -1 \\
\lim_{\xi \to L_0^-} T_{-2}(\xi) &= \lim_{\xi \to L_0^+} G_{-N}(\xi), \\
\lim_{\xi \to L_1^-} G_N(\xi) &= \lim_{\xi \to L_1^+} T_1(\xi), \\
\lim_{\xi \to L_0^-} K_w \partial_x T_{-2}(\xi) &= \lim_{\xi \to L_0^+} K_l \partial_x G_{-N}(\xi), \\
\lim_{\xi \to L_1^-} K_l \partial_x G_N(\xi) &= \lim_{\xi \to L_1^+} K_w \partial_x T_1(\xi).
\end{aligned}
$$

With the rest of the equations being

$$
\begin{aligned}
\lim_{\xi \to B_i^-} G_{i-1}(\xi) &= 0 \\
\lim_{\xi \to B_i^+} G_i(\xi) &= 0 \\
\lim_{\xi \to B_{-i}^-} G_{-i}(\xi) &= 0 \\
\lim_{\xi \to B_{-i}^+} G_{-i+1}(\xi) &= 0 \\
i &= 1, 2, \ldots, N
\end{aligned}
$$

This gives a total of $4N+8$ unknown quantities as well as $4N+8$ equations to solve for them. This system was solved by using a numerical root finding algorithm. An example of a solution on this form is give in figure 41